

This is to certify that the

thesis entitled

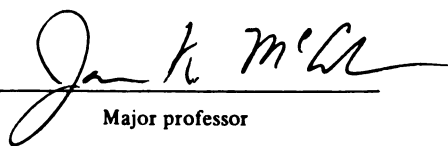
**Synthesis and Spectroscopy of Electron Exchange
Coupled Semiquinone Complexes of Chromium and Nickel**

presented by

Richard Tirasak Praseuth

has been accepted towards fulfillment
of the requirements for

M.S. degree in Chemistry


Major professor

Date 7/9/2002

LIBRARY
Michigan State
University

PLACE IN RETURN BOX to remove this checkout from your record.
TO AVOID FINES return on or before date due.
MAY BE RECALLED with earlier due date if requested.

DATE DUE	DATE DUE	DATE DUE
APR 17 2011		

SYNTHESIS AND SPECTROSCOPY OF ELECTRON EXCHANGE COUPLED
SEMIQUINONE COMPLEXES OF CHROMIUM AND NICKEL

By

Richard T. Praseuth

A THESIS

Submitted to
Michigan State University
in partial fulfillment of the requirements
for the degree of

MASTER OF SCIENCE

Department of Chemistry

2002

ABSTRACT

SYNTHESIS AND SPECTROSCOPY OF ELECTRON EXCHANGE COUPLED SEMIQUINONE COMPLEXES OF CHROMIUM AND NICKEL

By

Richard T. Praseuth

In this thesis, the impact of electron exchange coupling on the physical properties of nickel-semiquinone and chromium-semiquinone complexes is investigated. Following a brief discussion of magnetism in general, the synthesis, structure, and physical properties of $[\text{Ni}(\text{tren})(3,5\text{-DTBSQ})](\text{PF}_6)$ (where 3,5-DTBSQ is 3,5-di-*tert*-butylsemiquinone) are discussed. A group theoretical analysis demonstrates that the spin forbidden transition ${}^1\text{E} \leftarrow {}^3\text{A}_2$ transition in Ni^{II} should be altered due the presence of ferromagnetic coupling between Ni^{II} and a semiquinone ligand. In particular, it is shown that a transition from the ground state to the doublet low-lying excited state could be accomplished thermally. However, variable-temperature electronic absorption data failed to show the expected thermochromic effect. The magnetic properties of $\text{Cr}(3,5\text{-DTBSQ})_3$ and $\text{Cr}(\text{PhenSQ})_3$ are addressed to assess whether PhenSQ might couple more weakly to a metal ion and yield the thermochromic response that could not be achieved with the Ni-3,5-DTBSQ complex. In addition, the results of a density functional theory study of phenanthrenequinone and phenanthrenesemiquinone are discussed. The primary goals of this study were to explore the spatial distribution of the molecular orbitals and the relative ordering of energy levels of the molecular orbitals upon reduction from the quinone to the semiquinone redox state. Finally, future directions of this project are briefly discussed.

In loving memory of my grandmother, Judy Wong Sher.

ACKNOWLEDGEMENTS

First, I would like to take this opportunity to thank Professor James McCusker for all his support and guidance throughout the past two years at Michigan State University. In addition, I would like to thank the members of the McCusker Group; past and present. They have all been very helpful with my synthetic inquiries and great companions on the frequent trips down to Grand River (Grand Lake?) for lunch and coffee at Starbucks. Specifically, I would like to thank Jeff and Laura for reading and editing the multiple chapters of my thesis. Also, if it weren't for Jeff's expertise in x-ray crystallography, my thesis would have been void of any crystal structures and twenty pages shorter. Thank you very much Jeff.

Next, I would like to extend sincere thanks to Donna and Mike. You guys have been more than generous with me and over the past year or two, you guys have proven to be my "true" friends. Thank you very much for everything! You guys are great friends and you made life in East Lansing bearable. I will never forget the two of you. Furthermore, I would like to thank Javier for his friendship and willingness to skip work midday to play basketball with me. It was great playing ball with you and I hope we can do it again in the future.

Last, but not least, I would like to thank my family. I am very grateful for the encouragement and constant instilment of confidence in me to strive for my goals. I'm not sure what path I'll choose in the future but I'm confident that from the support and love given to me by my family, I will always be successful. Many thanks to my brothers (Mike, David, and Alex) for being the closest and best of friends to me. You guys have

been my role models since day one and the person I am today, good and bad, can be accredited to you guys. Thanks also to my sister-in-laws, Francine and Cheri, for being the sisters I've never had. I've enjoyed the many conversations we've had and semi-twisted humor we've shared.

TABLE OF CONTENTS

LIST OF TABLES.....	x
LIST OF FIGURES	xii
LIST OF ABBREVIATIONS.....	xvii

CHAPTER ONE: Synopsis of Electron Exchange Coupling and the Photophysics

of Transition Metal Complexes.....	1
1.1 Introduction.....	1
1.2 Definition of Electron Exchange Coupling.....	2
1.3 Determination of the Exchange Coupling Constant, J	3
1.4 Effects of Electron Exchange Coupling on Ground State Properties	7
1.5 Use of Quinones in Metal Compounds.....	8
1.6 Research Objectives.....	10
1.7 References and Notes.....	16

CHAPTER TWO: Electron Exchange and the Photophysical Properties of a

Nickel Monosemiquinone Complex: Synthesis and	
Spectroscopy.....	19
2.1 Introduction.....	19
2.2 Experimental Section.....	22
2.2.1 General.....	22

2.2.2	Synthesis of Ni(tren)Br ₂	22
2.2.3	Synthesis of [Ni(tren)(3,5-DTBSQ)](PF ₆).....	24
2.2.4	X-ray Structure Determination	24
2.2.5	Cyclic Voltammetry.....	25
2.2.6	Variable-Temperature Magnetic Susceptibility.....	30
2.3	Results and Discussion	30
2.3.1	Synthesis	30
2.3.2	Description of the X-Ray Structure of [Ni(tren)(3,5-DTBSQ)](PF ₆)	31
2.3.3	Electrochemistry	34
2.3.4	Magnetic Susceptibility	36
2.3.5	Electronic Absorption Spectra	42
2.4	Concluding Comments.....	44
2.5	References and Notes.....	47

CHAPTER THREE: Synthesis and Magnetic Properties of Cr(3,5-DTBSQ)₃ and

	Cr(PhenSQ)₃.....	49
3.1	Introduction.....	49
3.2	Experimental Section	50
3.2.1	General.....	50
3.2.2	Synthesis of Cr(3,5-DTBSQ) ₃	50
3.2.3	Synthesis of Cr(PhenSQ) ₃	51
3.2.4	Variable-Temperature Magnetic Susceptibility.....	51

3.3 Results and Discussion	51
3.3.1 Magnetism of Cr(3,5-DTBSQ) ₃	51
3.3.2 Magnetism of Cr(PhenSQ) ₃ and Comparison with Cr(3,5-DTBSQ) ₃	55
3.4 References and Notes.....	59

CHAPTER FOUR: Density Functional Theory Analysis of the Electronic Structures of Phenanthrenequinone and

Phenanthrenesemiquinone	61
4.1 Introduction.....	61
4.2 Computational Methods.....	63
4.2.1 General Methods.....	63
4.2.2 Geometry Optimizations.....	63
4.2.3 Single Point Calculations.....	64
4.3 Results and Discussion	67
4.3.1 Optimized Geometries of PhenQ and PhenSQ	67
4.3.2 Molecular Orbitals of Phenanthrenequinone (PhenQ).....	70
4.3.3 Molecular Orbitals of Phenanthrenesemiquinone (PhenSQ).....	76
4.3.4 Energy Spacing of the Molecular Orbitals of PhenQ and PhenSQ	79
4.3.5 Natural Population Analysis (NPA) Charge Densities and Spin Densities.....	81
4.4 Concluding Remarks.....	83

4.5 Future Directions	86
4.6 References.....	88

APPENDIX: Tables of Bond Lengths, Bond Angles, and Anisotropic Thermal Factors, for the Crystal Structure of [Ni(tren)(3,5-DTBSQ)](PF₆) Presented in Chapter 2	91
--	-----------

LIST OF TABLES

CHAPTER TWO:

Table 2.1. Crystal Data and Structure Refinement for [Ni(tren)(3,5-DTBSQ)](PF ₆)*AcOEt	26
Table 2.2. Atomic Coordinates [x 10 ⁴] and Equivalent Isotropic Displacement Parameters [Å ² x 10 ³] for [Ni(tren)(3,5-DTBSQ)](PF ₆).....	27
Table 2.3. Selected Bond Lengths and Bond Angles for [Ni(tren)(3,5-DTBSQ)](PF ₆)	32

CHAPTER FOUR:

Table 4.1. Total Self-Consistent Field Energies (Hartree) Obtained at the B3LYP/6-311G** Level Using the Optimized Geometries of PhenQ and PhenSQ.....	66
Table 4.2. Selected Optimized Bond Lengths (Å) for Phenanthrenequinone (PhenQ) and Phenanthrenesemiquinone (PhenSQ) Obtained from Self-Consistent Field (SCF) Geometry Optimizations at the B3LYP/6-31G* Level.....	69
Table 4.3. Energies and Percent Atomic Contributions to the Frontier Molecular Orbitals of Phenanthrenequinone (PhenQ) Obtained at the U-B3LYP/6-311G** Level	71

Table 4.4. Energies and Percent Atomic Contributions to the Frontier Molecular Orbitals of Phenanthrenesemiquinone (PhenSQ) Obtained at the U-B3LYP/6-311G** Level	77
Table 4.5. Absolute and Relative Orbital Energies (eV) of Phenanthrenequinone and Phenanthrenesemiquinone Calculated at the U-B3LYP/6-311G** Level	80
Table 4.6. NPA Atomic Charge Densities of Phenanthrenequinone and Phenanthrenesemiquinone Calculated at the U-B3LYP/6-311G** Level	82
Table 4.7. NPA Atomic Spin Densities and Mulliken Net Spin Densities for Phenanthrenequinone and Phenanthrenesemiquinone Obtained at the U-B3LYP/6-311G** Level	84

APPENDIX:

Table A.1. Bond Distances (Å) for [Ni(tren)(3,5-DTBSQ)](PF ₆)	92
Table A.2. Bond angles (°) for [Ni(tren)(3,5-DTBSQ)](PF ₆)	95
Table A.3. Anisotropic Displacement Parameters [Å ² x 10 ³] for [Ni(tren)(3,5-DTBSQ)](PF ₆). The Anisotropic Displacement Factor Exponent Takes the Form: $-2p2[(ha^*)2U11 + \dots + 2hka^*b^*U12]$	101

LIST OF FIGURES

CHAPTER ONE:

- Figure 1.1. Schematic representation of a two $S = \frac{1}{2}$ spin system in the absence and presence of electron exchange coupling. The electronic state ordering on the right is appropriate for an antiferromagnetically coupled system (i.e., $J < 0$).6
- Figure 1.2. The redox chemistry of quinones and spin states corresponding to the respective redox states9
- Figure 1.3. Examples of commonly studied *o*-semiquinone ligands:3,6-di-*tert*-butylquinone (3,6-DTBQ), 3,5-di-*tert*-butylquinone (3,5-DTBQ), tetrachloro-1,2-quinone (TCQ), 9,10-phenanthrenequinone (PhenQ)11
- Figure 1.4. Results of a ligand field analysis for a Cr(III)-quinone dyad applied by Wheeler et. al. The first column indicates two of the lowest-lying field states present in a d^3 metal ion in O_h symmetry. The second column represents the splitting upon lowering the symmetry from O_h to C_{2v} , which corresponds to $[\text{Cr}(\text{tren})(3,6\text{-DTBSQCat})]^+$. The third column represents the splitting caused by the coupling between the unpaired spins of the metal with an $S = \frac{1}{2}$ spin of b_1 symmetry. This corresponds to the complex, $[\text{Cr}(\text{tren})(3,6\text{-DTBSQ})]^{2+}$. The relative

ordering of the spin-coupled states for the Cr-SQ diagram assumes antiferromagnetic coupling in the excited states. Other higher-lying excited states that are present have been omitted for clarity13

Figure 1.5. Tanabe-Sugano diagram for a d^8 metal complex in octahedral symmetry.....14

CHAPTER TWO:

Figure 2.1. Room temperature absorption spectra of a) $[\text{Cr}(\text{tren})(3,6\text{-DTBCat})](\text{PF}_6)$ and b) $[\text{Cr}(\text{tren})(3,6\text{-DTBSQ})](\text{PF}_6)_2$ measured in 4:1 EtOH/MeOH.....21

Figure 2.2. Results of a ligand field analysis for a Ni(II)-quinone dyad. The first column indicates two of the lowest-lying ligand field states present in a d^8 metal ion in O symmetry. The second column represents the splitting upon lowering the symmetry from O to C_{2v} , which corresponds to a non-exchange coupled Ni(II) complex. The third column represents the splitting caused by the coupling between the unpaired spins of Ni(II) with the semiquinone ligand ($S = \frac{1}{2}$) of b_1 symmetry. This corresponds to the complex, $[\text{Ni}(\text{tren})(3,5\text{-DTBSQ})]^+$. Other higher-lying excited states that are present have been omitted for clarity23

Figure 2.3. Drawing and labeling scheme of the two crystallographically unique $[\text{Ni}(\text{tren})(3,5\text{-DTBSQ})]^+$ cations determined by single-crystal x-ray

diffraction. The structural and crystallographic details are summarized in Tables 2.1 through 2.3	33
Figure 2.4. Cyclic voltammogram of [Ni(tren)(3,5-DTBSQ)](PF ₆) in deaerated dichloromethane.....	35
Figure 2.5. The redox chemistry of [Ni(tren)(3,5-DTBSQ)] ⁺	37
Figure 2.6. Plot of effective magnetic moment versus temperature for [Ni(tren)(3,5-DTBSQ)](PF ₆) at 2.5 T with (squares) and without (triangles) the correction for temperature-independent paramagnetism (TIP).....	39
Figure 2.7 Schematic drawing of the effect of the zero-field splitting on the S = 3/2 ground state of [Ni(tren)(3,5-DTBSQ)] ⁺ . As drawn, D > 0; if D < 0, then the ± 3/2 levels would be lower in energy	41
Figure 2.8 Room-temperature absorption spectrum of [Ni(tren)(3,5-DTBSQ)](PF ₆) measured in dichloromethane	43
Figure 2.9 Variable-temperature electronic absorption spectra of [Ni(tren)(3,5-DTBSQ)](PF ₆) in dimethylformamide solution.....	45

CHAPTER THREE:

Figure 3.1. Plot of effective magnetic moment versus temperature for Cr(3,5-DTBSQ) ₃ (circles). The solid line represents the fit to a theoretical model; g = 2.00, TIP = 150 x 10 ⁻⁶ cm ³ /mol, and J = -440 cm ⁻¹	52
---	----

Figure 3.2. Energy levels for Cr(SQ) ₃ complexes resulting from intramolecular antiferromagnetic exchange between the unpaired electrons of the <i>o</i> -semiquinone ligands and the Cr(III) ion	56
Figure 3.3. Plots of effective magnetic moment versus temperature for Cr(PhenSQ) ₃ (circles) and Cr(3,5-DTBSQ) ₃ (triangles).....	58

CHAPTER FOUR:

Figure 4.1. Labeling scheme and coordinate system used for phenanthrenequinone and phenanthrenesemiquinone. The peripheral carbons are defined as C2, C3, C4, C5, C11, C12, C13, and C14.....	65
Figure 4.2. The redox states of phenanthrenequinone	68
Figure 4.3. MO 52 α of phenanthrenequinone. The orbital density is localized above and below the plane of the ring	72
Figure 4.4. MO 53 α of phenanthrenequinone. The orbital lies in the plane of the ring	72
Figure 4.5. MO 54 α (HOMO) of phenanthrenequinone. The orbital density lies above and below the plane of the ring	74
Figure 4.6. MO 55 α (LUMO) of phenanthrenequinone. The orbital density lies above and below the plane of the ring	74
Figure 4.7. MO 56 α of phenanthrenequinone. The orbital density lies above and below the plane of the ring.....	75
Figure 4.8. MO 55 α (HOMO) of phenanthrenesemiquinone. The orbital density lies above and below the plane of the ring.....	78

Figure 4.9. MO 55 β (LUMO) of phenanthrenesemiquinone. The orbital density
lies above and below the plane of the ring.....78

List of Abbreviations

3,5-DTBCat	3,5-di- <i>tert</i> -butylcatechol
3,5-DTBSQ	3,5-di- <i>tert</i> -butylsemiquinone
3,6-DTBSQ	3,6-di- <i>tert</i> -butylsemiquinone
AcOEt	Ethyl acetate
Cat	Catechol
CTH	5,7,7,12,14,14-hexamethyl-1,4,8,11-tetraazacyclodecane
DFT	Density functional theory
NPA	Natural population analysis
PhenSQ	9,10-phenanthrenesemiquinone
SCF	Self-consistent field
SQ	Semiquinone
TCSQ	Tetrachloro-1,2-semiquinone

CHAPTER ONE

Synopsis of Electron Exchange Coupling and the Physical Properties of Transition Metal Complexes

1.1 Introduction

For many years, chemists have been interested in understanding the physical properties, and ultimately the reactivity, of transition metal complexes. These properties can often be very complex and require an understanding of the electronic structure of the compound in question. One aspect of molecular electronic structure that has governed considerable attention relates to magnetism. In general, the arrangement of electrons in the valence orbitals of a molecule presents two types of magnetic behavior: paramagnetism or diamagnetism. The compound is defined as paramagnetic if it contains any unpaired electrons, whereas, if the electrons are all paired, the molecule is said to be diamagnetic. Depending on the type of complex, other factors may also be present, causing perturbations in the overall electronic structure. In addition, situations may arise where multiple paramagnetic centers are present in a single compound. To a large extent, the electronic structure of this type of system can be perturbed by the mutual interaction of the unpaired spins. The coupling between these spin centers, which occurs in the absence of any external field (e.g., magnetic or electronic), can vary in magnitude and the resulting physical properties of the chemical system will differ depending on the nature of the interaction.¹ This interaction (i.e., electron exchange coupling) has become an

increasingly important area of study for many disciplines of chemistry.²⁻⁷

1.2 Definition of Electron Exchange Coupling

Electron exchange coupling is an electrostatic interaction that arises whenever two or more paramagnetic centers are in close proximity. In order for this interaction to occur in any molecular system, two general criteria must be met: First, the complex must contain two or more species with unpaired electrons; Second, there must be a pathway through which the spins can interact. In addition, the spin orbitals must be reasonably similar energetically.⁸ The most common type of exchange observed is intramolecular exchange, which is exchange coupling between spin centers within the same molecule. This mode of coupling can occur via two mechanisms, either through direct overlap between the two spin centers or through a diamagnetic bridge, defined as “superexchange”.⁹ In the case of superexchange, a metal ion can act as the bridge, which provides a mode of interaction between the radical ligands. There are several examples of metal mediated coupling between radical ligands in the literature.¹⁰⁻¹² For example, Adams et. al.¹³ reported the synthesis and characterization of the gallium complex, $\text{Ga}(\text{3,5-DTBSQ})_3$ (3,5-DTBSQ = 3,5-di-*tert*-butylsemiquinone) which exhibits superexchange between the semiquinone ligands through the diamagnetic gallium(III) metal.

To a lesser extent, intermolecular exchange is also observed which is defined as exchange between separate molecules.^{14,15} Although this type of coupling occurs, it is quite often very weak. For example, complexes synthesized by Schulz et al.¹⁴ have shown

very weak intermolecular exchange coupling between separate Cu(II) centers mediated by hydrogen bonding. In general, intermolecular exchange coupling is orders of magnitude smaller than intramolecular exchange, and therefore will not be discussed further.

Another aspect of exchange that must be considered is the nature of spin alignment. This is a consequence of the details of the interactions between orbitals containing the unpaired electrons. If the electrons couple such that their spins are aligned antiparallel, the interaction is said to be antiferromagnetic. Orthogonality between magnetic orbitals, leading to a spin-aligned configuration is called a ferromagnetic interaction.⁵ This difference in coupling and the resulting perturbations in the physical properties of the compound will be discussed further in the following sections.

1.3 Determination of the Exchange Coupling Constant, J

The basis of understanding how exchange coupling affects the properties of a system requires knowledge concerning the strength of the interaction between the spin centers. In general, the coupling can be described by the spin Hamiltonian (\mathbf{H})¹⁶ of the form shown in Equation 1.1, where \mathbf{S}_i and \mathbf{S}_j represent the quantum mechanical

$$\mathbf{H} = -2 \sum_i \sum_j J_{ij} \mathbf{S}_i \cdot \mathbf{S}_j \quad (1.1)$$

spin operators on the i^{th} and j^{th} paramagnetic site, and J is the exchange coupling constant which quantifies the magnitude of the coupling between the spin centers. Based

on Equation 1.1, a negative value of J represents an antiferromagnetically coupled system (spins are aligned antiparallel), whereas a positive value represents a ferromagnetic system (spins are aligned parallel).

A simple but illustrative example of exchange coupling can be envisioned between two paramagnetic centers, each with $S = \frac{1}{2}$. Based on Equation 1.1, the Hamiltonian that describes this system is given below in Equation 1.2.

$$\mathbf{H} = -2 J_{12} \mathbf{S}_1 \cdot \mathbf{S}_2 \quad (1.2)$$

Using the Kambe approximation¹⁷ and defining the total spin of the complex, \mathbf{S}_T , as $\mathbf{S}_T = \mathbf{S}_1 + \mathbf{S}_2$, an operator-equivalent form of Equation 1.2 can be derived (Equation 1.3).

$$\mathbf{H} = -J_{12} [\mathbf{S}_T^2 - \mathbf{S}_1^2 - \mathbf{S}_2^2] \quad (1.3)$$

From Equation 1.3, the corresponding eigenvalue expression can be generated, Equation 1.4, and the two eigenvalues ($E_{S_T=0}$ and $E_{S_T=1}$) can be easily obtained as $+1.5 J$ and $-0.5 J$,

$$E(S) = -J [\mathbf{S}_T(\mathbf{S}_T+1) - \mathbf{S}_1(\mathbf{S}_1+1) - \mathbf{S}_2(\mathbf{S}_2+1)] \quad (1.4)$$

respectively. The energy that separates the two states is given in Equation 1.5.

$$\Delta E = E(S_T=0) - E(S_T=1) = 1.5J - (-0.5J) = 2J \quad (1.5)$$

The resulting energy levels (i.e., spin ladder) are shown in Figure 1.1. The left side of the figure depicts two $S = \frac{1}{2}$ spin centers prior to exchange interactions. The two possible spin interactions, $S_T = 0$ and $S_T = 1$, are degenerate prior to coupling. Upon introduction of exchange coupling interactions, the degeneracy of the spins, $S_T = 0$ and $S_T = 1$, is removed and the states are separated by $2J$ (the energies of these electronic states are given by Equation 1.4).

For molecular systems, the magnitude of exchange coupling (J) is often determined by measuring the bulk magnetization of a sample as a function of temperature. Magnetic susceptibility is determined from a Boltzmann distribution over the available spin states of the system. The general expression for magnetic susceptibility is given by Equation 1.6.¹⁸ This can be further simplified to a more useful form, given in Equation 1.7¹⁸, where N is Avogadro's number, g is the gyromagnetic factor of the electron, β is the electron Bohr magneton, k_B is the Boltzmann constant, T is temperature, S is the total spin quantum number of a given spin state, and $E(S)$ is the energy associated with that spin state (e.g., Equation 1.4). The summation is made over all the spin states in the system.

$$\chi = \frac{Ng^2\beta^2 \sum_S \sum_{M_S=-S}^S M_S^2 \exp[-E(S)/k_B T]}{k_B T \sum_S (2S + 1) \exp[-E(S)/k_B T]} \quad (1.6)$$

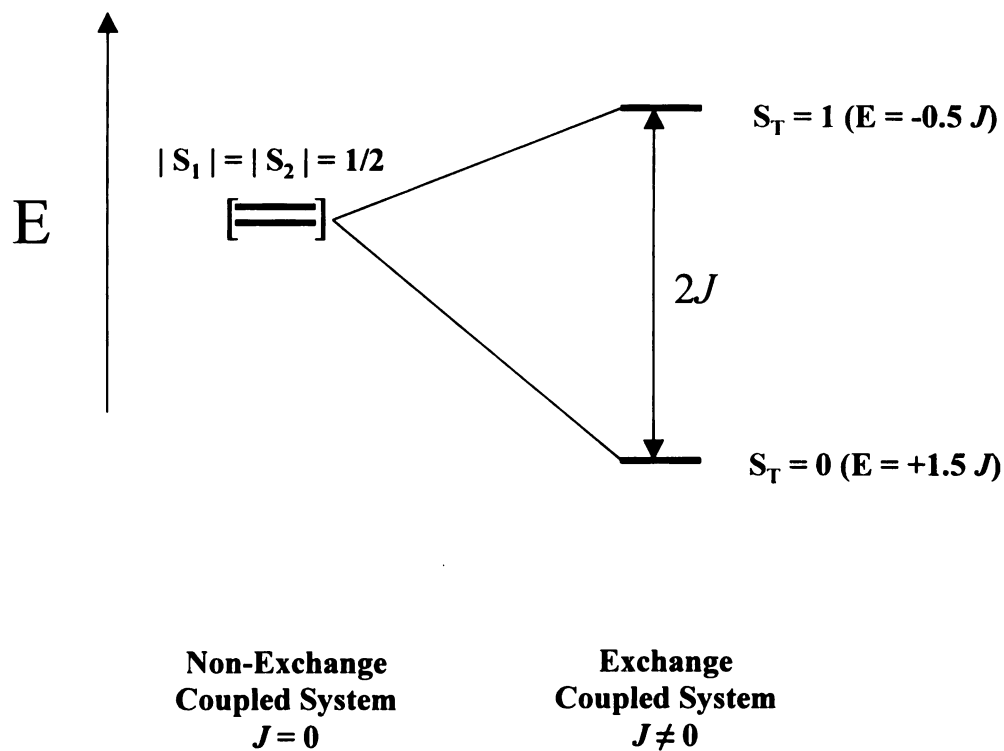


Figure 1.1. Schematic representation of a two $S = \frac{1}{2}$ spin system in the absence and presence of exchange coupling. The electronic state ordering on the right is appropriate for an antiferromagnetically coupled system (i.e., $J < 0$).

$$\chi = \frac{N g^2 \beta^2 \sum_S S(S+1)(2S+1) \exp[-E(S)/k_B T]}{3 k_B T \sum_S (2S+1) \exp[-E(S)/k_B T]} \quad (1.7)$$

The variable temperature magnetic susceptibility data obtained from experiment can then be fit to Equations 1.6 or 1.7 to obtain a value for the exchange coupling constant, J .¹⁹

1.4 Effects of Electron Exchange Coupling on Ground State Properties

As mentioned above, a molecule's physical properties are largely determined by its electronic structure. This can be altered dramatically by the introduction of exchange interactions, which will manifest themselves in the ground state properties of the complex. The most obvious effect can be observed in the magnetism of these complexes. For example, in the absence of exchange coupling, a molecule which contains two high spin Fe(III) centers should have a magnetic moment²⁰ of approximately $8.37 \mu_B$. The magnetic moment can deviate substantially if the two metals are coupled. Our group has found that two antiferromagnetically coupled Fe(III) metal centers bridged by an oxo group, can exhibit an effective magnetic moment of $2.45 \mu_B$ (at 300K) as seen in the complex $\text{Fe}_2\text{O}(\text{O}_2\text{CCH}_2\text{F})_2(\text{Tp})_2$ (Tp = 1-hydro(trispyrazolyl)borate).²¹ This demonstrates the dramatic effect of an interaction that is nominally ca. 100 cm^{-1} in magnitude.

The absorptive properties of a molecular complex can also be perturbed by exchange interactions. In the high spin non-exchange coupled Fe(III) dinuclear cluster mentioned above, the ground state of each Fe(III) atom in octahedral geometry would be

6A_1 . By examination of the Tanabe-Sugano²² diagram, it is clear that there are no spin-allowed ligand-field transitions from the ground state. However, upon the introduction of exchange coupling, the overall spin states of both the ground state and the excited states of the system are altered. Therefore, it is possible for excitations which were formally forbidden in the absence of exchange to become allowed upon introduction of exchange coupling interactions.

1.5 Use of Quinones in Model Compounds

Quinones have attracted interest from a number of researchers because of their “non-innocent” behavior as ligands with respect to their oxidation states. In general, quinones possess three stable oxidation states in which the semiquinone redox state is paramagnetic with $S = \frac{1}{2}$ (Figure 1.2). A large number of complexes containing quinones have been synthesized and exploited as models to study the effects of electron exchange coupling on the physical properties of molecules. The type of exchange-coupled systems studied have varied from simple complexes consisting of a paramagnetic metal ion chelated by a single semiquinone ligand²³⁻²⁶ to diamagnetic metals chelated by multiple semiquinone ligands^{11,12,27}. A third type of system, which is more complicated, consists of multiple semiquinone ligands chelated to a paramagnetic metal ion²⁸⁻³⁰. This type of system involves two modes of exchange; direct exchange between the metal and the semiquinone ligands, and superexchange between the semiquinone ligands.⁵

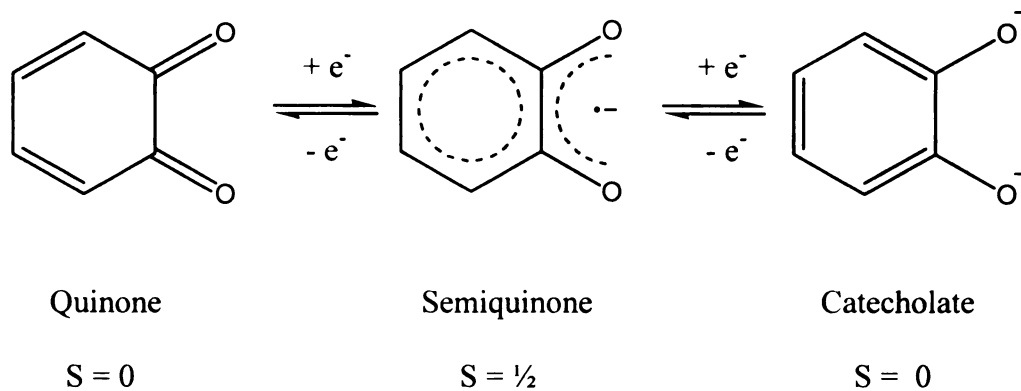
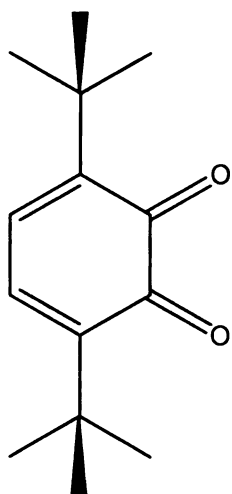


Figure 1.2. The redox chemistry of quinones and spin states corresponding to the respective redox states.

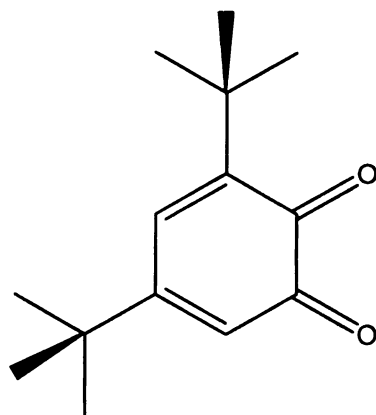
The advantage of using a redox-active ligand such as a quinone lies in the ability to effectively turn exchange coupling on or off in a given system without making substantial changes in the overall composition of the molecule. This can be accomplished by oxidizing the catecholate ligand ($S = 0$) to the semiquinone form ($S = 1/2$).³¹ A few examples of the widely studied ortho-quinone ligands are listed in Figure 1.3.

1.6 Research Objectives

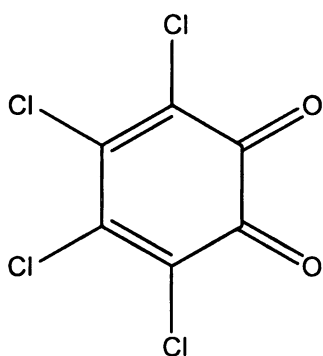
Previous studies have investigated the effects of exchange coupling on the spectroscopic properties of Cr^{III}-semiquinone^{23,24} and Cr^{III}-catecholate systems.²³ These systems represent excellent models for the systematic study of the effect of electron exchange coupling on the physical and photophysical properties of metal complexes. Focusing on [Cr(tren)(3,6-DTBSQ)]²⁺, where tren is tris-2-(aminoethyl)amine, complex, the magnetic susceptibility data confirmed the presence of antiferromagnetic coupling between the metal and the semiquinone ligand.²³ A qualitative ligand-field theory analysis of the electronic structure applied by Wheeler et al. to both the catecholate and semiquinone complexes accounted for the optical properties of the semiquinone complex. The ground state of the catecholate complex was found to be ⁴B₂, which splits into ³A₂ and ⁵A₂ upon introduction of electron exchange with the semiquinone. This is illustrated in Figure 1.4, along with the term states of the Cr^{III} - catechol complex in C_{2v} symmetry



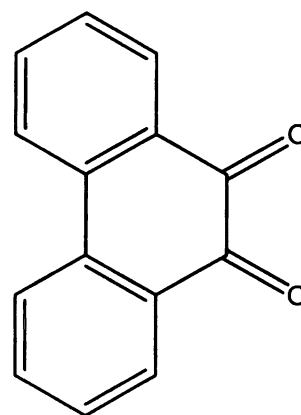
3,6-DTBQ



3,5-DTBQ



TCQ



PhenQ

Figure 1.3. Examples of commonly studied *o*-quinone ligands: 3,6-di-*tert*-butylquinone (3,6-DTBQ), 3,5-di-*tert*-butylquinone (3,5-DTBQ), tetrachloro-1,2-quinone (TCQ), 9,10-phenanthrenequinone (PhenQ).

and their parent terms in O_h .²⁴ Essentially, electron exchange interactions between Cr(III)-SQ creates two new transitions (${}^3A_2 \leftarrow {}^3A_2$, z-polarized, and ${}^3B_1 \leftarrow {}^3A_2$, y-polarized) from the ground state that were formally spin forbidden in the catecholate complex.²³

Examination of the Tanabe-Sugano diagram²² of a d^8 metal ion in octahedral symmetry (Figure 1.5) reveals that the ground state of Ni(II) is 3A_2 with a low-lying 1E excited state. Given the fact that nickel(II)-semiquinone complexes are known to exhibit strong ferromagnetic interactions^{32,33} between the metal and semiquinone ligand, it should be possible to produce spin allowed transitions analogous to the Cr(III)-semiquinone complexes but from thermally accessed excited states.

In this thesis, the impact of electron exchange coupling on the physical properties of nickel-semiquinone and chromium-semiquinone complexes is investigated. Specifically, the idea of thermochromism that arises as a result of exchange interactions is probed. The model complexes that will be used to study this feature are Ni(II)-semiquinone complexes. In Chapter Two, the synthesis and physical properties of $[\text{Ni}(\text{tren})(3,5\text{-DTBSQ})](\text{PF}_6)$ are presented. Variable-temperature electronic absorption spectroscopy was used as a probe for the detection of thermochromism. As mentioned earlier, the ground state of Ni^{II} is 3A_2 with a low-lying 1E state. The transition from the ground state to the 1E excited state is formally spin forbidden but the presence of ferromagnetic coupling between Ni^{II} and a semiquinone ligand should produce a spin allowed transition analogous to the $[\text{Cr}(\text{tren})(3,6\text{-DTBSQ})]^{2+}$ complex but from a thermally-accessed excited state. This idea of thermochromism will be explored in Chapter 2.

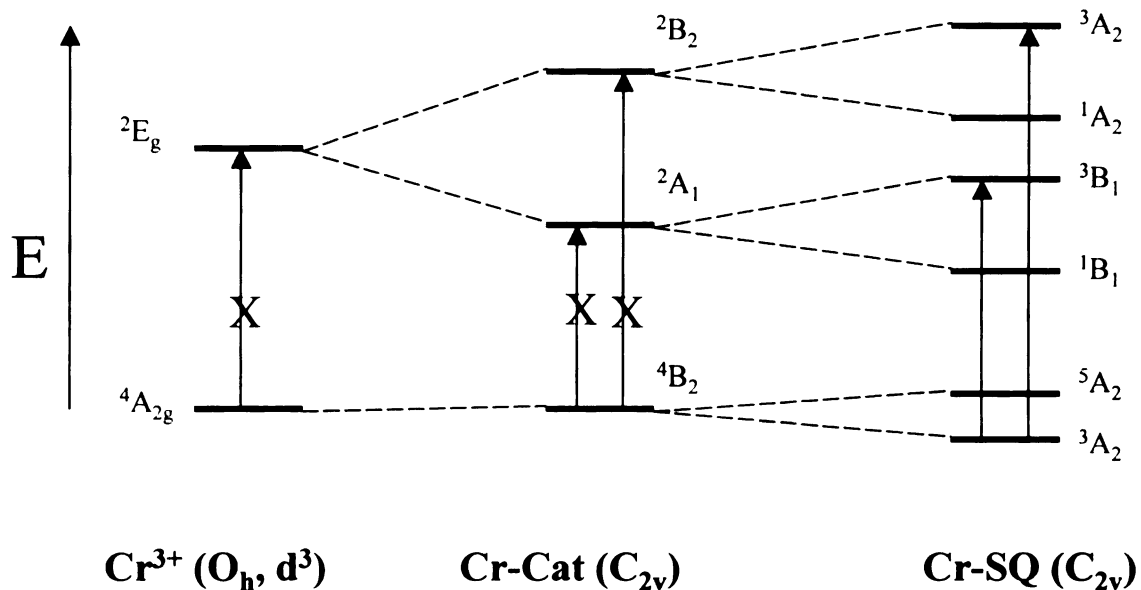


Figure 1.4. Results of a ligand field analysis for a Cr(III)-quinone dyad applied by Wheeler et al.²⁴. The first column indicates two of the lowest-lying ligand field states present in a d^3 metal ion in O_h symmetry. The second column represents the splitting upon lowering the symmetry from O_h to C_{2v} , which corresponds to $[\text{Cr}(\text{tren})(3,6\text{-DTBCat})]^+$. The third column represents the splitting caused by the coupling between the unpaired spins of the metal with an $S = \frac{1}{2}$ spin of b_1 symmetry. This corresponds to the complex, $[\text{Cr}(\text{tren})(3,6\text{-DTBSQ})]^{2+}$. The relative ordering of the spin-coupled states for the Cr-SQ diagram assumes antiferromagnetic coupling in the excited states. Other higher-lying excited states that are present have been omitted for clarity.

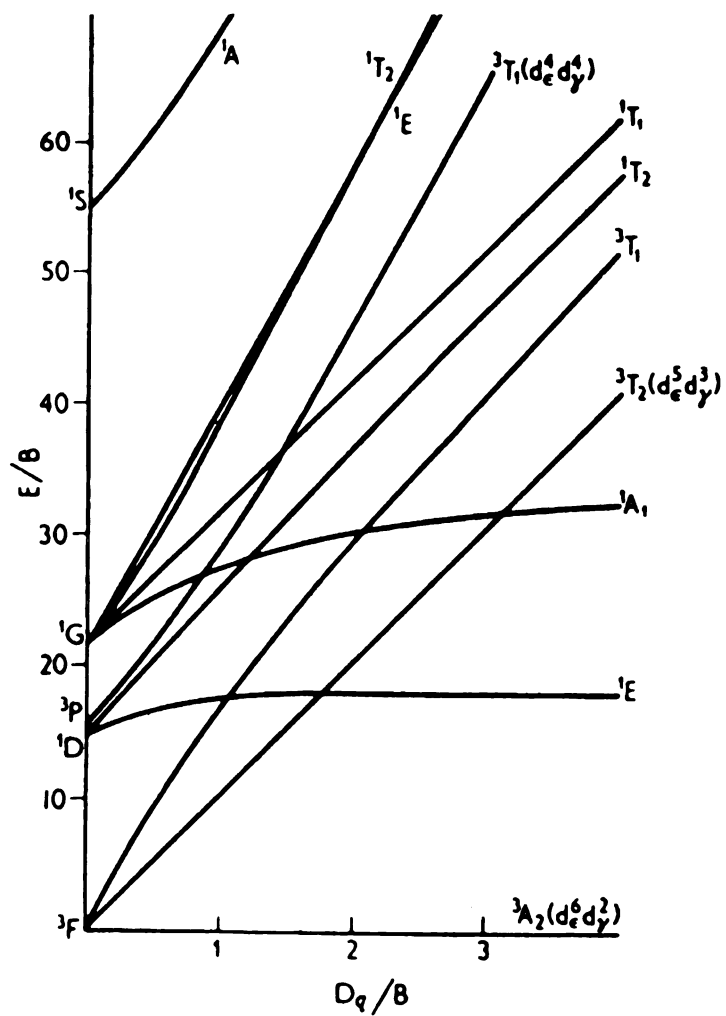


Figure 1.5. Tanabe-Sugano diagram for a d^8 metal complex in octahedral symmetry.²²

In Chapter Three, the magnetic properties of $\text{Cr}(3,5\text{-DTBSQ})_3$ and $\text{Cr}(\text{PhenSQ})_3$ are described. This study was performed in search of a semiquinone ligand that couples more weakly to a metal ion than 3,5-DTBSQ. The magnitude of exchange coupling for $\text{Cr}(3,5\text{-DTBSQ})_3$ was determined and compared with the value known for the complex $\text{Cr}(\text{PhenSQ})_3$. These data provide an indication of the relative strength of interaction of the two semiquinones to the same metal center, in this case Cr(III). The relative magnitudes of the coupling constants between Ni(II) and these semiquinone ligands could then be inferred given similar geometric environments.

In Chapter Four, the results of an ab-initio density functional theory study performed on phenanthrenequinone and phenanthrenesemiquinone are discussed. The primary goals of this study were to explore the spatial distribution of the molecular orbitals and the relative ordering of energy levels of the molecular orbitals upon reduction from the quinone to the semiquinone redox state. In addition, the results found in this study are compared to those found for 3,5-di-*tert*-butylquinone, providing insight into the differences between the two quinones. Finally, future directions of this project will be discussed briefly.

1.7 References and Notes

- (1) The coupling between the two unpaired spins can either be ferromagnetic or antiferromagnetic which can result in significant differences in the physical properties (e.g., magnetism) of the system.
- (2) Schugar, H. J.; Rossman, G. R.; Barraclogh, C. G.; Gray, H. B. *J. Am. Chem. Soc.* **1972**, *94*, 100.
- (3) Stenkamp, R. E.; Sieker, L. C.; Jensen, L. H. *J. Mol. Biol.* **1978**, *126*, 457.
- (4) Sheriff, S.; Hendrickson, W. A.; Smith, J. L. *J. Mol. Biol.* **1987**, *197*, 273.
- (5) Pierpont, C. G.; Attia, A. S. *Collect. Czech. Chem. Commun.* **2001**, *66*, 33.
- (6) Miller, J. S.; Epstein, A. J.; Reiff, W. M. *Acc. Chem. Res.* **1988**, *21*, 114.
- (7) Iwamura, H. *Adv. Phys. Org. Chem.* **1990**, *26*, 179.
- (8) Thoman, M.; Kahn, O.; Guilheim, J.; Varret, F. *Inorg. Chem.* **1994**, *33*
- (9) Hay, P. J.; Thibeault, J. C.; Hoffman, R. *J. Am. Chem. Soc.* **1975**, *97*, 4884.
- (10) Bhattacharya, S.; Pierpont, C. G. *Inorg. Chem.* **1994**, *33*, 6038.
- (11) Lange, C. W.; Pierpont, C. G. *Inorg. Chim. Acta.* **1997**, *263*, 219.
- (12) Lange, C. W.; Conklin, B. J.; Pierpont, C. G. *Inorg. Chem.* **1994**, *33*, 1276.
- (13) Adams, D. M.; Rheingold, A. L.; Dei, A.; Hendrickson, D. N. *Angew. Chem., Int. Ed. Engl.* **1994**, *32*, 391.
- (14) Schulz, D.; Weyhermuller, T.; Wieghardt, K.; Butzlaff, C.; Trautwein, A. X. *Inorg. Chim. Acta.* **1996**, *246*, 387.
- (15) Tosik, A.; Maniukiewicz, W.; Bukowska-Strzyzewska, M.; Mrozinski, J.; Sigalas, M. P.; Tsipis, C. A. *Inorg. Chim. Acta.* **1991**, *190*, 193.

- (16) Ginsberg, A. P. *J. Am. Chem. Soc.* **1980**, *102*, 111.
- (17) Kambe, K. *J. Phys. Soc. Jpn.* **1950**, *48*, 5.
- (18) Kahn, O. *Molecular Magnetism* New York, NY, 1993.
- (19) Parameters for paramagnetic impurities and temperature-independent paramagnetism (TIP) are included in the determination of J .
- (20) The effective magnetic moment of two non-interacting spins can be calculated using the equation, $\mu_{\text{eff}} = [n_1(n_1+2) + n_2(n_2+2)]^{1/2}$ (n_i = number of unpaired electrons).
- (21) Weldon, B. T.; Wheeler, D. E.; Kirby, J. P.; McCusker, J. K. *Inorg. Chem.* **2001**, *40*, 6802.
- (22) Tanabe, Y.; Sugano, S. *J. Phys. Soc. Japan* **1954**, *753*, 766.
- (23) Wheeler, D. E.; McCusker, J. K. *Inorg. Chem.* **1998**, *37*, 2296.
- (24) Benelli, C.; Dei, A.; Gatteschi, D.; Gudel, H.; Pardi, L. *Inorg. Chem.* **1989**, *28*, 3089.
- (25) Kessel, S. L.; Emberson, R. M.; Debrunner, P. G.; Hendrickson, D. N. *Inorg. Chem.* **1980**, *19*, 1170.
- (26) Ruf, M.; Noll, B. C.; Groner, M. D.; Yee, G. T.; Pierpont, C. G. *Inorg. Chem.* **1997**, *36*, 4860.
- (27) Bruni, S.; Caneschi, A.; Cariati, F.; Delfs, C.; Dei, A.; Gatteschi, D. *J. Am. Chem. Soc.* **1994**, *116*, 1388.
- (28) Buchanan, R. M.; Kessel, S. L.; Downs, H. H.; Pierpont, C. G.; Hendrickson, D. N. *J. Am. Chem. Soc.* **1978**, *100*, 7894.

- (29) Attia, A. S.; Conklin, B. J.; Lange, C. W.; Pierpont, C. G. *Inorg. Chem.* **1996**, *35*, 1033.
- (30) Lynch, M. W.; Buchanan, R. M.; Pierpont, C. G.; Hendrickson, D. N. *Inorg. Chem.* **1981**, *20*, 1038.
- (31) Further oxidation to the quinone redox state is not desirable because the quinone binds very weakly to metal ions and would readily dissociate.
- (32) Benelli, C.; Dei, A.; Gatteschi, D.; Pardi, L. *Inorg. Chem.* **1988**, *27*, 2831.
- (33) Benelli, C.; Dei, A.; Gatteschi, D.; Pardi, L. *Inorg. Chem.* **1989**, *28*, 1476.

CHAPTER TWO

Synthesis and Physical Properties of a Nickel-Monosemiquinone Complex

2.1 Introduction

A large number of complexes containing a single radical semiquinone ligand chelated to a paramagnetic metal ion have been studied. In general, they all exhibit strong exchange interactions between the metal ion and semiquinone ligand. Previous studies have investigated the effects of exchange coupling on the spectroscopic properties of Cr^{III}-semiquinone and Cr^{III}-catecholate systems.^{1,2} These systems represent excellent models for the systematic study of the effect of electron exchange coupling on the physical and photophysical properties of metal complexes. Benelli and co-workers¹ were the first to report such a complex in 1989 in which the synthesis, magnetic, and electronic absorption properties of [Cr(CTH)(3,5-DTBSQ)]²⁺ (CTH = 5,7,7,12,14,14-hexamethyl-1,4,8,11-tetraazacyclodecane) were reported. Later, our group developed a related dyad system using 3,6-DTBSQ and the tetradentate capping ligand, tris-(2-aminoethyl)amine (tren).² In addition, the non-exchange coupled catecholate analogue, [Cr(tren)(3,6-DTBCat)]⁺, was synthesized for comparison.² These compounds and their physical properties were extensively characterized. Magnetic data revealed the presence of strong antiferromagnetic coupling in [Cr(tren)(3,6-DTBSQ)]²⁺, however, the most pronounced perturbation was observed in the absorption spectrum (Figure 2.1). The semiquinone

complex exhibited additional peaks in the absorption spectrum which were absent in the non-exchange coupled catecholate complex. These peaks were qualitatively accounted for using a simple group theoretical analysis. The ground state of the catecholate complex is 4B_2 . Upon introduction of electron exchange in the semiquinone complex, this state splits into 3A_2 and 5A_2 with the 3A_2 term lying lowest in energy. This effectively creates two new transitions (${}^3A_2 \leftarrow {}^3A_2$ and ${}^3B_1 \leftarrow {}^3A_2$) from the ground state which were formally spin forbidden in the catecholate complex.²

By analogy, an extension of this study can be made using Ni(II). An examination of the Tanabe-Sugano diagram of a d^8 metal ion in octahedral symmetry, as seen in Figure 1.4, reveals that the ground state of Ni(II) is 3A_2 with a low-lying 1E excited state. Pseudooctahedral nickel(II) complexes have been found to couple ferromagnetically to semiquinone ligands.^{3,4} The difference in coupling between Cr-SQ and Ni-SQ can be rationalized in terms of the molecular orbitals involved. MO calculations have shown that the single unpaired electron in *o*-semiquinones resides in a π -type molecular orbital.⁵⁻⁷ In pseudooctahedral complexes, the metal e_g orbitals are considered σ -antibonding orbitals while the metal t_{2g} orbitals are of the π -antibonding type. It follows, then, that the chromium(III)-SQ complexes would be expected to exhibit an antiferromagnetic exchange interaction because one of the three unpaired electrons of the Cr(III) metal resides in an orbital having the same symmetry as the magnetic orbital of the semiquinone ligand.⁸ In contrast, the σ -type magnetic orbitals of the Ni(II) ion are orthogonal to that of the semiquinone ligand, giving rise to ferromagnetic coupling in the Ni(II)-SQ system. This was the result found by Benelli et al.³ for $[Ni(CTH)(3,5-DTBSQ)]^+$.

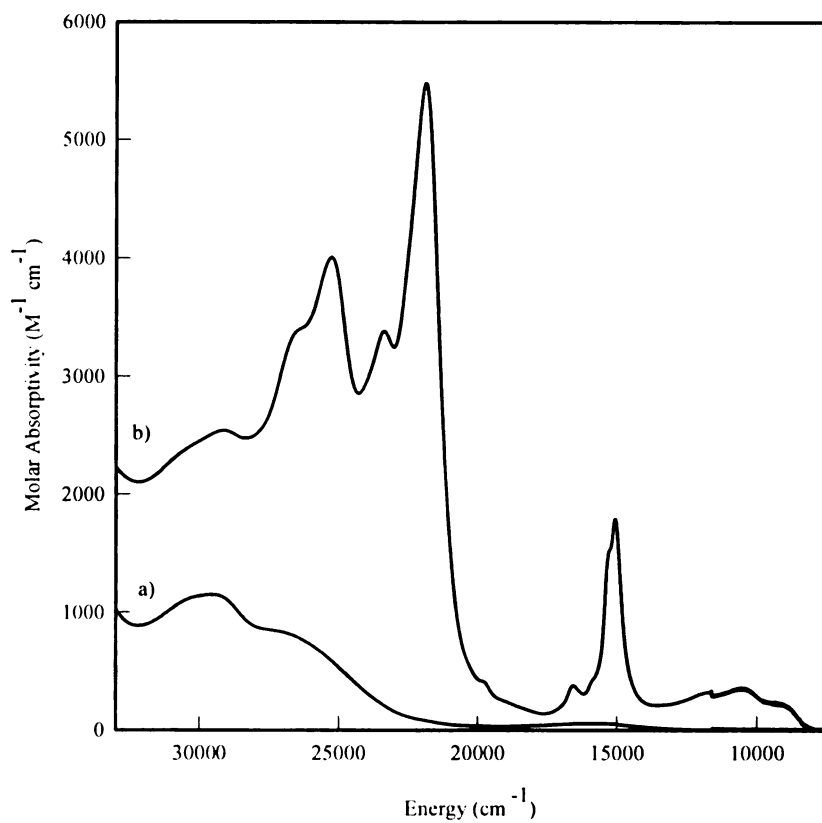


Figure 2.1. Room temperature absorption spectra² of a) $[\text{Cr}(\text{tren})(3,6\text{-DTBCat})](\text{PF}_6)$ and b) $[\text{Cr}(\text{tren})(3,6\text{-DTBSQ})](\text{PF}_6)_2$ measured in 4:1 EtOH/MeOH.

In terms of optical properties, spin-allowed transitions analogous to the Cr(III)-semiquinone complexes should be possible as a result of exchange coupling in the Ni-SQ complex. However, due to the ferromagnetic coupling, this transition will originate from the higher lying term of the ground-state spin ladder. A schematic diagram is shown in Figure 2.2. If the doublet state (2A_2) formed by exchange interactions is thermally accessible, the compound should be thermochromic.

2.2. Experimental Section

2.2.1. General

All reagents and materials were obtained from commercial sources and were used as received except for the ligand tris(2-aminoethyl)amine (tren), which was vacuum distilled prior to use. Solvents were purchased from either Aldrich Chemical Co. or Strem. Elemental analysis was obtained through the Analytical Facilities of Michigan State University.

2.2.2. Synthesis of Ni(tren)Br₂

This compound was prepared by a method analogous to that reported previously for Ni(tren)Cl₂.⁹ Tren (0.350 g, 2.40 mmol) was dissolved in 95% ethanol (25 mL) and placed into a 125 mL round bottom flask. NiBr₂ · xH₂O (0.500 g, 2.30 mmol) was added to the tren solution and the resulting blue solution was stirred for one hour. The volume

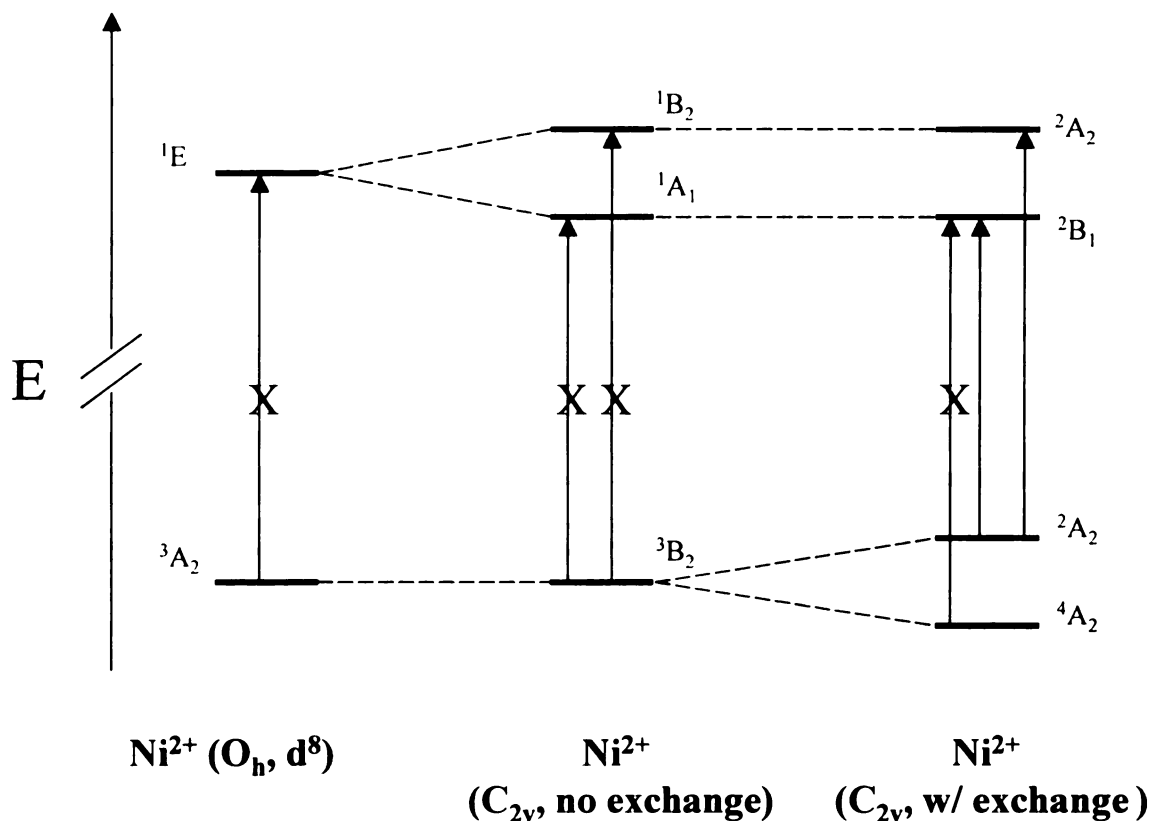


Figure 2.2. Results of a ligand field analysis for a Ni(II)-quinone dyad. The first column indicates two of the lowest-lying ligand field states present in a d⁸ metal ion in O symmetry. The second column represents the splitting upon lowering the symmetry from O to C_{2v}, which corresponds to a non-exchange coupled Ni(II) complex. The third column represents the splitting caused by the coupling between the unpaired spins of Ni(II) with the semiquinone ligand (S = 1/2) of b₁ symmetry. This corresponds to the complex, [Ni(tren)(3,5-DTBSQ)]⁺. Other higher-lying excited states that are present have been omitted for clarity.

of the solution was reduced to ca. 5 mL by rotary evaporation and the resulting blue solid was collected by filtration and washed with absolute ethanol (3 x 25 mL).

2.2.3. Synthesis of [Ni(tren)(3,5-DTBSQ)](PF₆)

The following synthesis is a slight modification of the method reported by Benelli et al.³ In an inert atmosphere box, 3,5-DTBQ (0.100 g, 0.450 mmol) was reduced to 3,5-DTBCat by addition of excess Na metal to a solution of the quinone in THF (10 mL). This solution was then filtered and cannulated over to a solution of Ni(tren)Br₂ (0.165 g, 0.450 mmol) dissolved in degassed methanol (25 mL). The resulting solution was stirred for 1 h at room temperature and then removed from the glovebox, whereupon an immediate color change from light violet to dark brown was noted. The volume of the solution was reduced to approximately 5 mL by rotary evaporation followed by addition of a saturated aqueous solution of excess potassium hexafluorophosphate which induced the precipitation of a black-green solid. The solid was collected and redissolved in dichloromethane. The product was precipitated by addition of hexanes to this dichloromethane solution and isolated by filtration. Yield: 0.187 g (72.8%). Anal. Calcd for NiC₂₀O₂N₄H₃₈PF₆: C, 42.13; H, 6.72; N, 9.83. Found: C, 42.15; H, 6.74; N, 9.40.

2.2.4. X-ray Structure Determination

A single-crystal x-ray structure determination of [Ni(tren)(3,5-DTBSQ)](PF₆) was carried out at the x-ray facility of the Department of Chemistry, Michigan State

University by Dr. Jeffrey Bodwin. A blue block crystal of $[\text{Ni}(\text{tren})(3,5\text{-DTBSQ})](\text{PF}_6)$ was obtained by layering hexanes onto an ethyl acetate solution of the compound. One crystal having approximate dimensions of 0.35 x 0.20 x 0.12 mm was mounted on a glass fiber. Diffraction data were collected on a Siemens SMART diffractometer with graphite monochromated Mo K α X-ray radiation. Data were collected at 173 K. Details of crystal and experimental data are given in Table 2.1, and positional parameters are listed in Table 2.2. Cell parameters were obtained from 8996 independent reflections in the range $1.74^\circ < \theta < 23.29^\circ$. Absorption corrections were performed using SAD.ABS. The structural parameters were refined by using version 5.1 SHELXTL package.¹⁰ Disorder present in the PF_6^- anions, ethyl acetate solvates, and carbons 15 and 16 within the capping tren ligand, were modelled as two components in each case and the occupancies independently refined. The final least-squares refinement, performed by introducing hydrogen atoms in idealized positions, converged with $R = 0.0543$ ($R_w = 0.1430$).

2.2.5 Cyclic Voltammetry

Electrochemical measurements were carried out inside an N_2 -filled glovebox using a BAS CV-50W electrochemical analyzer. The compound was dissolved in distilled and deaerated CH_2Cl_2 containing NBu_4PF_6 (ca. 0.1 M) as the supporting electrolyte. A standard three-electrode setup was used with a platinum working electrode, platinum wire counter electrode, and a Ag/AgNO_3 electrode as reference. The voltammogram was recorded at a scan rate of 100 mV/s. The reported potentials can be

Table 2.1 Crystal Data and Structure Refinement for [Ni(tren)(3,5-DTBSQ)](PF₆)*AcOEt

Empirical formula	C ₂₄ H ₄₆ F ₆ N ₄ Ni ₁ O ₄ P ₁	
Formula weight	526.66	
Temperature (K)	173(2)	
Wavelength (Å)	0.71073	
Crystal system	Triclinic	
Space group	P $\bar{1}$	
Unit cell dimensions	a = 11.954(2) Å	alpha = 100.85(3)°
	b = 12.090(2) Å	beta = 97.01(3)°
	c = 22.489(5) Å	gamma = 98.65(3)°
Volume (Å ³)	3117.7(11)	
Z	5	
Density (calculated) (Mgm ³)	1.403	
Absorption coefficient (mm ⁻¹)	0.744	
F(000)	1388	
Crystal size (mm)	0.35 x 0.20 x 0.12	
q range for data collection (deg)	1.74 to 23.29	
Limiting indices	-13 < h < 13, -13 < k < 13, -25 < l < 24	
Reflections collected	27106	
Independent reflections	8996 (R _{int} = 0.0900)	
Completeness to q = 23.29°	99.90%	
Refinement method	Full-matrix least-squares on F ²	
Data / restraints / parameters	8996 / 0 / 832	
Goodness-of-fit on F ²	1.034	
Final R indices [I > 2s(I)]	R1 = 0.0543, wR ² = 0.1430	
R indices (all data)	R1 = 0.0680, wR ² = 0.1529	
Largest diff. peak and hole (eÅ ⁻³)	0.892 and -0.546	

Table 2.2. Atomic Coordinates [x 10⁴] and Equivalent Isotropic DisplacementParameters [$\text{\AA}^2 \times 10^3$] for [Ni(tren)(3,5-DTBSQ)](PF₆).

	x	y	z	U (eq) ^a
Ni(1)	854(1)	3789(1)	-1797(1)	26(1)
O(1)	-222(2)	2844(2)	-2586(1)	31(1)
O(2)	1647(2)	4422(2)	-2438(1)	29(1)
C(1)	140(3)	3096(3)	-3068(2)	24(1)
C(2)	1184(3)	3940(3)	-2987(2)	25(1)
C(3)	1635(3)	4185(3)	-3522(2)	26(1)
C(4)	1032(3)	3634(3)	-4085(2)	29(1)
C(5)	-3(3)	2817(3)	-4172(2)	27(1)
C(6)	-431(3)	2568(3)	-3666(2)	27(1)
C(7)	2758(3)	5036(3)	-3449(2)	31(1)
C(8)	3731(3)	4606(4)	-3094(2)	40(1)
C(9)	2620(4)	6225(3)	-3106(2)	40(1)
C(10)	3116(4)	5173(4)	-4067(2)	47(1)
C(11)	-573(3)	2239(3)	-4827(2)	30(1)
C(12)	-1609(4)	1319(4)	-4834(2)	49(1)
C(13)	-977(4)	3125(4)	-5163(2)	47(1)
C(14)	283(4)	1661(4)	-5174(2)	43(1)
N(1)	94(2)	3108(2)	-1125(1)	27(1)
N(3)	1716(3)	2381(3)	-1833(1)	34(1)
N(4)	-452(3)	4796(3)	-1742(1)	35(1)
N(2)	1925(17)	4807(16)	-1063(9)	36(8)
C(15)	670(20)	3680(20)	-472(15)	22(5)
C(16)	1371(9)	4872(9)	-503(4)	38(3)
N(2')	1995(19)	4876(15)	-1036(10)	30(7)
C(15')	730(20)	3780(30)	-556(16)	37(9)
C(16')	1937(8)	4321(9)	-534(4)	34(3)
C(17)	199(3)	1882(3)	-1246(2)	39(1)
C(18)	1390(4)	1733(3)	-1370(2)	41(1)

^aU(eq) is defined as 1/3 of the trace of the orthogonalized U_{ij} tensor.

Table 2.2. continued

	x	y	z	U (eq)
C(19)	-1121(3)	3267(3)	-1221(2)	36(1)
C(20)	-1193(3)	4473(3)	-1295(2)	39(1)
Ni(2)	3634(1)	2231(1)	1599(1)	26(1)
O(11)	4414(2)	1642(2)	2327(1)	31(1)
O(12)	2992(2)	3124(2)	2294(1)	32(1)
C(21)	4113(3)	2090(3)	2839(2)	25(1)
C(22)	3315(3)	2898(3)	2815(2)	25(1)
C(23)	2934(3)	3393(3)	3378(2)	27(1)
C(24)	3380(3)	3100(3)	3902(2)	30(1)
C(25)	4171(3)	2330(3)	3936(2)	27(1)
C(26)	4524(3)	1840(3)	3406(2)	27(1)
C(27)	2071(3)	4202(3)	3358(2)	34(1)
C(28)	960(3)	3590(4)	2932(2)	45(1)
C(29)	2586(4)	5256(3)	3126(2)	43(1)
C(30)	1767(4)	4624(4)	3994(2)	57(1)
C(31)	4584(3)	2085(3)	4565(2)	32(1)
C(32)	5232(4)	3182(4)	4997(2)	59(1)
C(33)	5388(4)	1214(5)	4521(2)	63(2)
C(34)	3568(4)	1594(4)	4840(2)	54(1)
N(11)	4266(3)	1243(3)	895(1)	33(1)
N(12)	2334(3)	785(3)	1434(2)	41(1)
N(13)	5227(3)	3332(3)	1684(2)	40(1)
N(14)	2882(3)	2905(3)	893(2)	43(1)
C(35)	3868(4)	49(3)	946(2)	48(1)
C(36)	2592(4)	-148(4)	969(2)	58(1)
C(37)	5520(3)	1567(4)	1039(2)	45(1)
C(38)	5881(4)	2847(4)	1215(2)	48(1)
C(39)	3826(4)	1496(4)	298(2)	48(1)
C(40)	2791(6)	2021(6)	329(2)	87(2)
P(1)	9215(1)	11862(1)	819(1)	38(1)
F(1)	8663(4)	12453(5)	324(2)	137(2)
F(2)	9722(3)	11119(3)	309(2)	109(1)
F(3)	9776(3)	11293(3)	1317(2)	99(1)
F(4)	10361(2)	12793(2)	928(2)	82(1)
F(5)	8097(3)	10942(3)	717(2)	91(1)

Table 2.2. continued

	x	y	z	U (eq)
F(6)	8738(2)	12671(2)	1330(2)	73(1)
P(2)	4831(1)	6483(1)	1124(1)	78(1)
F(11)	4204(8)	5869(12)	1675(6)	120(4)
F(12)	5642(17)	5830(30)	774(13)	243(13)
F(13)	3922(14)	7268(11)	1220(11)	165(11)
F(14)	5593(11)	6480(30)	1702(9)	170(9)
F(15)	5670(11)	7568(16)	1069(9)	121(6)
F(16)	4127(17)	5553(19)	722(7)	201(12)
F(11')	5565(11)	7501(18)	1627(17)	252(14)
F(12')	5734(9)	5748(13)	1317(11)	119(6)
F(13')	4059(13)	7010(20)	1475(7)	190(11)
F(14')	3933(13)	5359(11)	932(10)	151(8)
F(15')	5492(16)	6750(30)	667(12)	230(11)
F(16')	4168(8)	6679(11)	470(5)	137(5)
O(51)	2061(4)	-563(4)	2357(2)	103(2)
O(52)	2843(3)	-915(3)	3234(2)	64(1)
C(51)	1459(5)	233(5)	3279(3)	77(2)
C(52)	2136(5)	-444(4)	2902(3)	62(1)
C(53)	3513(6)	-1628(7)	2866(4)	104(2)
C(54)	4469(8)	-1748(9)	3191(6)	276(10)
O(53)	7365(4)	614(3)	3580(2)	75(1)
C(55)	7703(5)	-1285(5)	3572(3)	73(2)
C(56)	7745(4)	-207(5)	3353(2)	57(1)
O(54)	8395(4)	-174(6)	2901(3)	33(2)
C(57)	8481(9)	809(8)	2634(4)	40(3)
C(58)	7432(9)	900(10)	2233(5)	44(3)
O(54')	7810(60)	-420(30)	2772(12)	189(16)
C(57')	7180(30)	470(30)	2379(16)	124(13)
C(58')	8270(40)	1130(30)	2550(30)	240(40)

converted from reference to Ag/AgNO₃ to SCE by comparison to ferrocene measured under identical conditions.¹¹

2.2.6 Variable-Temperature Magnetic Susceptibility

Magnetic susceptibility data were collected using a Quantum Design MPMS SQUID magnetometer interfaced to an IBM PC. The apparatus was calibrated by measuring the magnetic susceptibility of [(CH₃)₂NHCH₂CH₂NH(CH₃)₂]CuCl₄¹² at several temperatures between 5 and 380 K. Data were collected at two magnetic field strengths of 1T and 2.5T and corrected for diamagnetism using Pascal's constants.¹³

2.3 Results and Discussion

2.3.1. Synthesis

Previous studies of the Cr-SQ dyad [Cr(tren)(3,6-DTBSQ)](PF₆)₂ by our group led us to the idea of studying a related Ni-SQ dyad. A thorough search of the literature yielded only two examples of this motif for nickel(II).^{3,4} Benelli, et al.^{3,4} reported the synthesis and characterization of [Ni(CTH)(3,5-DTBQ)]Y (Y = ClO₄, PF₆, BPh₄) and [Ni(CTH)(TCSQ)](ClO₄), where 3,5-DTBSQ is 3,5-di-tert-butylorthoquinone, TCSQ is 3,4,5,6-tetrachloroorthoquinone, and CTH is 5,7,7,12,14,14-hexamethyl-1,4,8,11-tetraazacyclodecane, a tetradentate macrocycle. The system involving the 3,5-DTBSQ radical seemed to be a reasonable starting point for our research. The synthesis

of the title compound involves cannulation of a THF solution of 3,5-DTBCat to a methanol solution of Ni(tren)Br₂ followed by air oxidation. A black-green material was obtained by reducing the volume of the solution to approximately 5 mL followed addition of a saturated aqueous solution of KPF₆. The solid obtained analyzed satisfactorily for [Ni(tren)(3,5-DTBSQ)](PF₆).

2.3.2. Description of the X-ray Structure of [Ni(tren)(3,5-DTBSQ)](PF₆)

[Ni(tren)(3,5-DTBSQ)](PF₆) crystallizes as an ethyl acetate solvate in the triclinic space group P $\bar{1}$. The unit cell is comprised of two crystallographically unique [Ni(tren)(3,5-DTBSQ)] cations, two PF₆⁻ anions, and two ethyl acetate solvates. The crystallographic details are given in Table 2.1, with positional parameters and bond distances and angles given in Tables 2.2 and 2.3, respectively. Additional details of the structure are found in the appendix. An ORTEP drawing of the cation is depicted in Figure 2.3, which confirms the monomeric nature of [Ni(tren)(3,5-DTBSQ)](PF₆). The geometry of the compound is best described as a distorted octahedron with the nickel coordinated by four aliphatic nitrogen atoms from the tren and two oxygen donors from the *o*-semiquinone. The Ni-N bond distances are all different; Ni(1)-N(3) and Ni(1)-N(4) at 2.113(3) and 2.120(3) Å, respectively, are significantly longer than the Ni(1)-N(1) and Ni(1)-N(2) bonds (2.091(3) and 2.032(19), respectively). The Ni-O bond distances, Ni(1)-O(1) and Ni(1)-O(2) are 2.085(3) Å and 2.022(2) Å, respectively. These values compare well with those reported by Benelli et. al. for [Ni(CTH)(3,5-DTBSQ)]⁺.³

Table 2.3. Selected Bond Lengths and Bond Angles for [Ni(tren)(3,5-DTBSQ)](PF₆)

Bond Lengths (Å)			
Ni(1)-O(2)	2.022(2)	Ni(1)-O(1)	2.085(3)
Ni(1)-N(1)	2.091(3)	Ni(1)-N(2)	2.032(19)
Ni(1)-N(3)	2.113(3)	Ni(1)-N(4)	2.120(3)
O(1)-C(1)	1.286(4)	O(2)-C(2)	1.279(4)
C(1)-C(2)	1.458(5)	C(1)-C(6)	1.415(5)
C(2)-C(3)	1.438(5)	C(3)-C(4)	1.372(5)
C(4)-C(5)	1.430(5)	C(5)-C(6)	1.369(5)
Ni(2)-O(11)	2.079(2)	Ni(2)-O(12)	2.025(2)
Ni(2)-N(11)	2.088(3)	Ni(2)-N(12)	2.099(3)
Ni(2)-N(13)	2.119(3)	Ni(2)-N(14)	2.086(3)
O(11)-C(21)	1.294(4)	O(12)-C(22)	1.278(4)
C(21)-C(22)	1.468(5)	C(21)-C(26)	1.412(5)
C(22)-C(23)	1.453(5)	C(23)-C(24)	1.363(5)
C(24)-C(25)	1.429(5)	C(25)-C(26)	1.371(5)
Bond Angles (deg)			
O(2)-Ni(1)-N(2)	95.8(6)	O(12)-Ni(2)-O(11)	80.52(9)
O(2)-Ni(1)-O(1)	80.49(9)	O(12)-Ni(2)-N(14)	97.78(12)
N(2)-Ni(1)-O(1)	175.7(6)	O(11)-Ni(2)-N(14)	177.18(12)
O(2)-Ni(1)-N(1)	177.64(11)	O(12)-Ni(2)-N(11)	177.43(11)
N(2)-Ni(1)-N(1)	83.2(6)	O(11)-Ni(2)-N(11)	98.00(11)
O(1)-Ni(1)-N(1)	100.54(11)	N(14)-Ni(2)-N(11)	83.78(13)
O(2)-Ni(1)-N(3)	94.62(11)	O(12)-Ni(2)-N(12)	95.07(12)
N(2)-Ni(1)-N(3)	95.6(6)	O(11)-Ni(2)-N(12)	88.60(12)
O(1)-Ni(1)-N(3)	86.94(11)	N(14)-Ni(2)-N(12)	93.80(14)
N(1)-Ni(1)-N(3)	83.33(12)	N(11)-Ni(2)-N(12)	82.77(13)
O(2)-Ni(1)-N(4)	99.37(11)	O(12)-Ni(2)-N(13)	98.82(12)
N(2)-Ni(1)-N(4)	94.7(5)	O(11)-Ni(2)-N(13)	85.16(12)
O(1)-Ni(1)-N(4)	83.77(11)	N(14)-Ni(2)-N(13)	92.91(14)
N(1)-Ni(1)-N(4)	82.87(12)	N(11)-Ni(2)-N(13)	83.11(13)
N(3)-Ni(1)-N(4)	161.66(12)	N(12)-Ni(2)-N(13)	163.61(13)

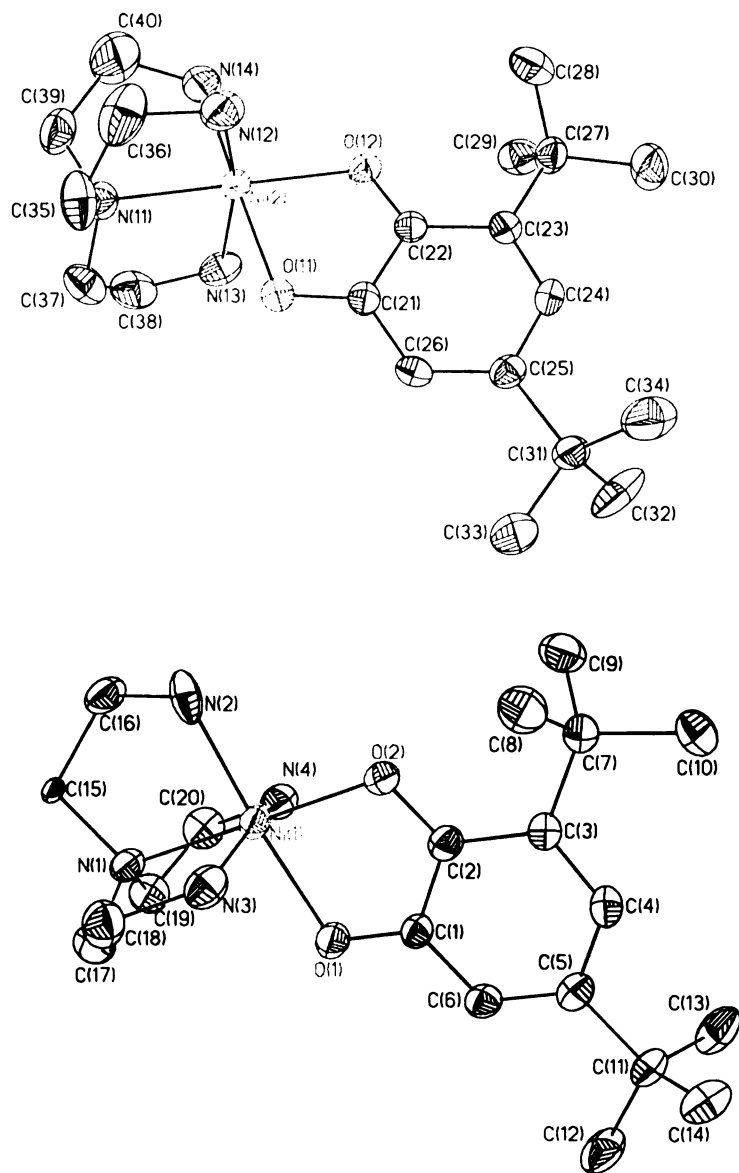


Figure 2.3. Drawing and labeling scheme of the two crystallographically unique $[\text{Ni}(\text{tren})(3,5\text{-DTBSQ})]^+$ cations determined by single-crystal x-ray diffraction. The structural and crystallographic details are summarized in Tables 2.1 through 2.3.

Overall, however, the local symmetry around the Ni(II) can still be reasonably approximated as C_{2v} .

Given the empirical formula, charge balance clearly requires an oxidation state of -1 for this ligand. However, the oxidation state of the *o*-quinone bound to the metal is also apparent by examining the bond lengths within the ring of the ligand.¹⁴ In general, in the catecholate form all the C-C bond distances are nearly identical due to the aromatic nature of the ligand. In contrast, the semiquinone redox state exhibits alternating short and long C-C bond distances because of the more localized nature of the double bonds within the ring. Given this, the semiquinone redox state is clearly evident. For example, C(3)-C(4) and C(5)-C(6) are found to be 1.372(5) Å and 1.369(5) Å, respectively, whereas C(1)-C(2), C(2)-C(3), C(4)-C(5), and C(1)-C(6) are all on average 1.435 ± 0.005 Å. The C-O bond distances also support the semiquinone redox state, with C(1)-O(1) and C(2)-O(2) distances of 1.286(4) and 1.279(4) Å, respectively. The shorter C(2)-O(2) bond suggests more double-bond character than the C(1)-O(1) bond. However, these differences are only marginal given the standard deviations quoted.

2.3.3. Electrochemistry

The cyclic voltammogram of a deaerated dichloromethane solution of [Ni(tren)(3,5-DTBSQ)](PF₆), depicted in Figure 2.4, reveals two redox couples at -0.739 and $+0.104$ V (vs Ag/AgNO₃). The two redox processes can be reasonably attributed to the SQ⁻¹/Cat²⁻ and Q⁰/SQ⁻¹ couples based on several considerations. First, the oxidation and reduction processes involving the nickel(II) ion are expected to occur at significantly

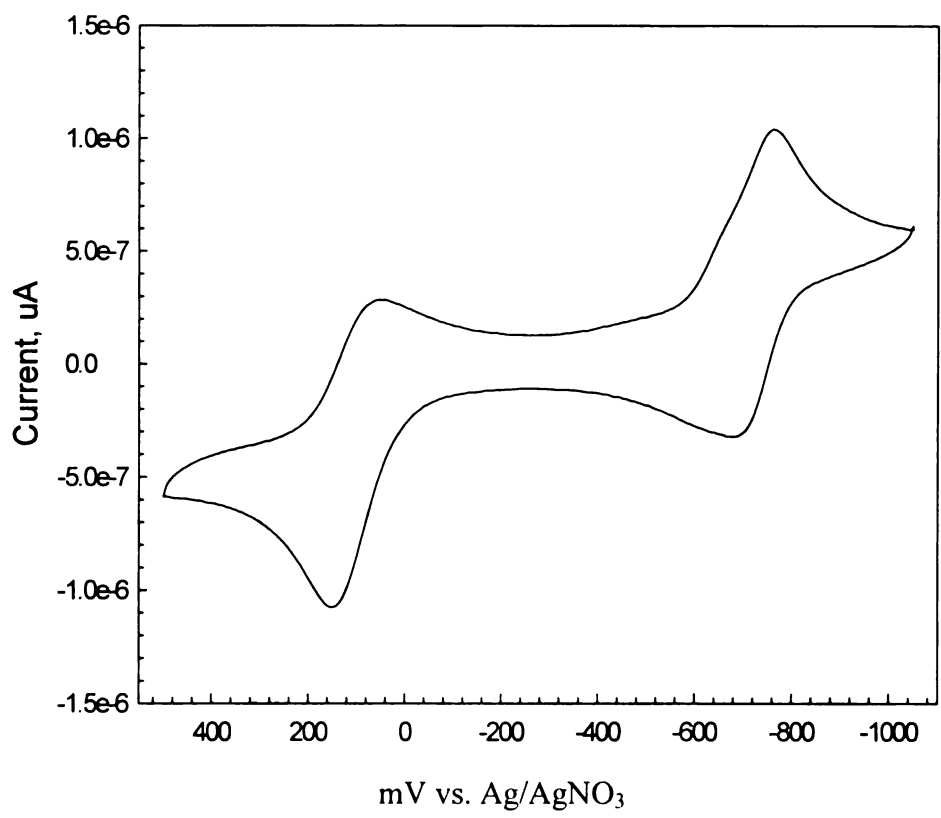


Figure 2.4. Cyclic voltammogram of $[\text{Ni}(\text{tren})(3,5\text{-DTBSQ})](\text{PF}_6)$ in deaerated dichloromethane.

more positive or more negative potentials, respectively.^{15,16} Second, the cyclic voltammogram of 3,5-DTBSQ¹⁷ in acetonitrile exhibits a redox couple corresponding to 3,5-DTBQ \rightarrow 3,5-DTBSQ at -0.955 V vs Ag/AgNO₃. Finally, these potentials are similar to those observed for the analogous Cr^{III} complex. The one-electron wave at -0.739 V is reversible with a peak separation of 66 mV, whereas the one-electron wave at 0.104 V is at best quasi-reversible. This is not surprising due to the fact that the fully oxidized quinone is expected to be a weakly binding ligand. Formation of this species following oxidation of the semiquinone complex will likely result in ligand dissociation, hence an irreversible wave in the cyclic voltammogram. This hypothesis is supported by the fact that the oxidation wave becomes more reversible at faster scan rates. The overall redox chemistry of [Ni(tren)(3,5-DTBSQ)](PF₆) is summarized in Figure 2.5. A shoulder seen in the second wave is attributed to the reduction of free quinone which is liberated from the complex upon oxidation of [Ni(tren)(3,5-DTBSQ)]⁺ to [Ni(tren)(3,5-DTBQ)]²⁺.

2.3.4. Magnetic Susceptibility

Electron exchange within the ground state configuration of this class of molecules can be quantified by variable-temperature magnetic susceptibility measurements. Electron exchange in low-symmetry complexes can be described using a simple Heisenberg exchange Hamiltonian of the form in Equation 2.1,

$$\mathbf{H} = -2 \sum_i \sum_j J_{ij} \mathbf{S}_i \cdot \mathbf{S}_j \quad (2.1)$$

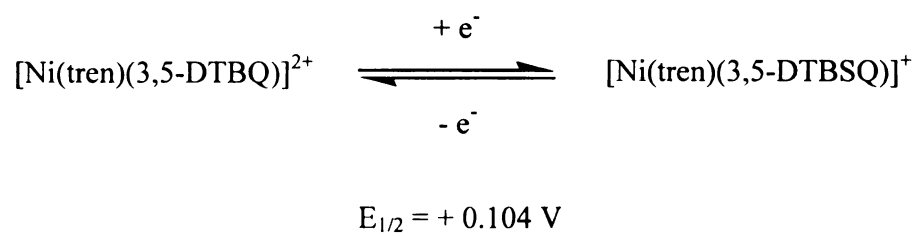
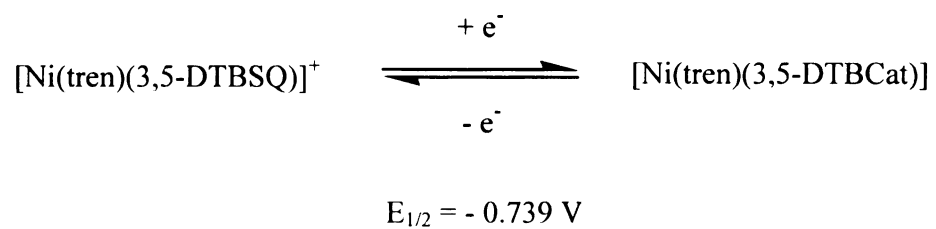


Figure 2.5. The redox chemistry of $[\text{Ni}(\text{tren})(3,5\text{-DTBSQ})]^+$.

where S_i and S_j represent the quantum mechanical spin operators on the i^{th} and j^{th} (e.g., the Ni^{II} ion and the semiquinone radical) paramagnetic site respectively. J_{ij} is the exchange coupling constant, a scalar quantity which gauges the magnitude of the coupling between the spin centers. Defining the total spin of the system, S_T , as $S_T = S_1 + S_2$ and using the Kambe approximation¹⁸ the operator-equivalent expression given in Equation 2.2 can be derived,

$$\mathbf{H} = -J [S_T^2 - S_1^2 - S_2^2] \quad (2.2)$$

and the data analyzed as described in Chapter 1.

Variable temperature data were collected at magnetic field strengths of 1 T and 2.5 T. A Plot of the effective magnetic moment versus temperature in the range from 5 - 380 K for solid samples of $[\text{Ni}(\text{tren})(3,5\text{-DTBSQ})](\text{PF}_6)$ is given in Figure 2.6 (data at 2.5 T). In addition, the data were corrected for temperature-independent paramagnetism¹⁹ and shown in these figures.

At 2.5 T and 380 K, the effective magnetic moment is $3.57 \mu_B$ and approaches $3.83 \mu_B$ at 100 K, which is a value close to the $S = 3/2$ moment ($\mu_{\text{eff}} = 3.87 \mu_B$) expected for a ferromagnetically coupled nickel(II)-SQ dyad. The magnetic moment then decreases to a value of $3.67 \mu_B$ at 10 K and continues to decline. The decline in effective moment at room temperature from the $S = 3/2$ moment is due to the population of the doublet excited state, 2A_2 and suggests that the exchange constant, J , is on the order of a couple of hundred wavenumbers.

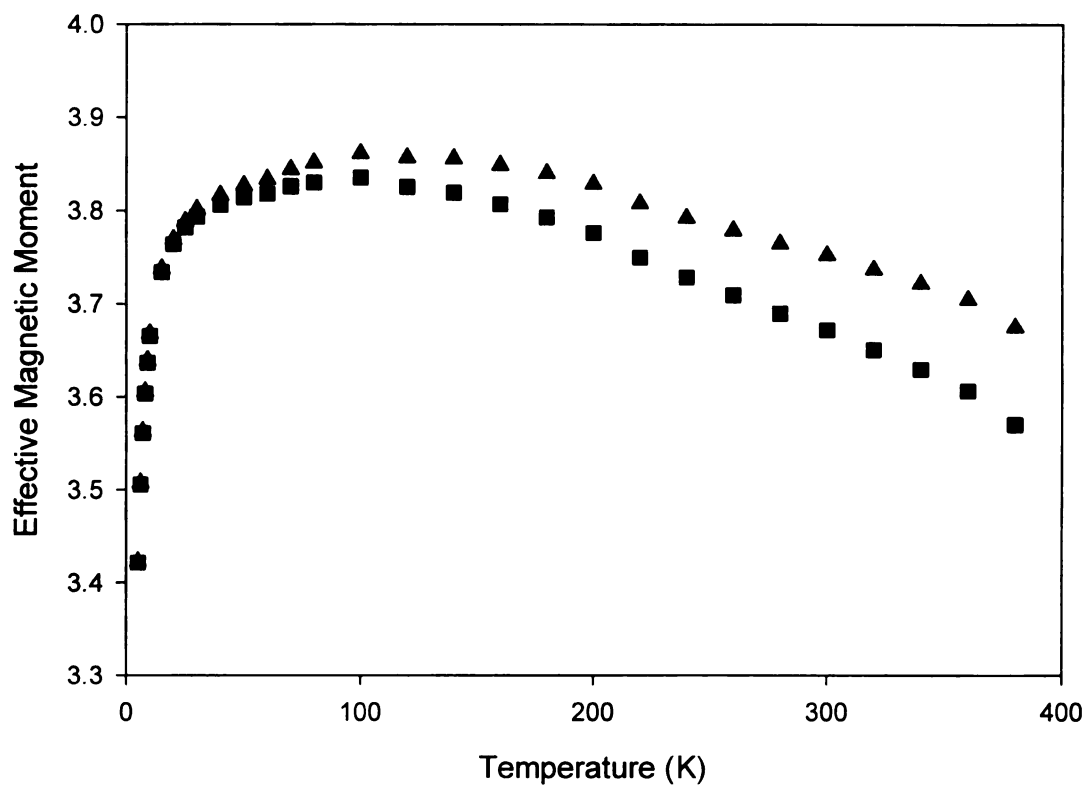


Figure 2.6. Plot of effective magnetic moment versus temperature for [Ni(tren)(3,5-DTBSQ)](PF₆) at 2.5 T with (squares) and without (triangles) the correction for temperature-independent paramagnetism (TIP).

The drop in μ_{eff} below 100 K can be explained by considering the phenomenon of zero-field splitting. A diagram which illustrates the effect of zero-field splitting of the $S = 3/2$ state of $[\text{Ni}(\text{tren})(3,5\text{-DTBSQ})]^+$ is presented in Figure 2.7. Based on symmetry and the degeneracy the point group (C_{2v}) can support, the fourfold degeneracy of the $S = 3/2$ state, ($m_S = \pm 1/2, \pm 3/2$), is partially lifted with the $m_S = \pm 3/2$ and $\pm 1/2$ levels separated by an amount $2D$. The zero-field parameter, D , not only has magnitude but also sign. As drawn, $D > 0$; if < 0 , then the $\pm 3/2$ levels would be lower in energy. From Figure 2.5 and 2.6, we can infer that D is positive in the case of $[\text{Ni}(\text{tren})(3,5\text{-DTBSQ})](\text{PF}_6)$ because the effective magnetic moment drops significantly below the value expected for $S = 3/2$.

Due to the presence of zero-field splitting, the Hamiltonian presented in Equation 2.1 must be adjusted to include this effect. In the case of $[\text{Ni}(\text{tren})(3,5\text{-DTBSQ})](\text{PF}_6)$, the Hamiltonian becomes

$$\mathbf{H} = -J[\mathbf{S}_T^2 - \mathbf{S}_1^2 - \mathbf{S}_2^2] + D[\mathbf{S}_Z^2 - 1/3\mathbf{S}_T^2] \quad (2.2)$$

where D is the zero-field splitting parameter and \mathbf{S}_Z is the m_S value of the sublevel. The magnetic data indicates that the zero-field splitting parameter is quite large due to the appearance of zero-field splitting effects at approximately 80 K. This result suggests that D is comparable enough in magnitude to J so as to make questionable the use of the Van Vleck equation to fit the data. A full matrix approach to analyzing these data is currently being pursued.

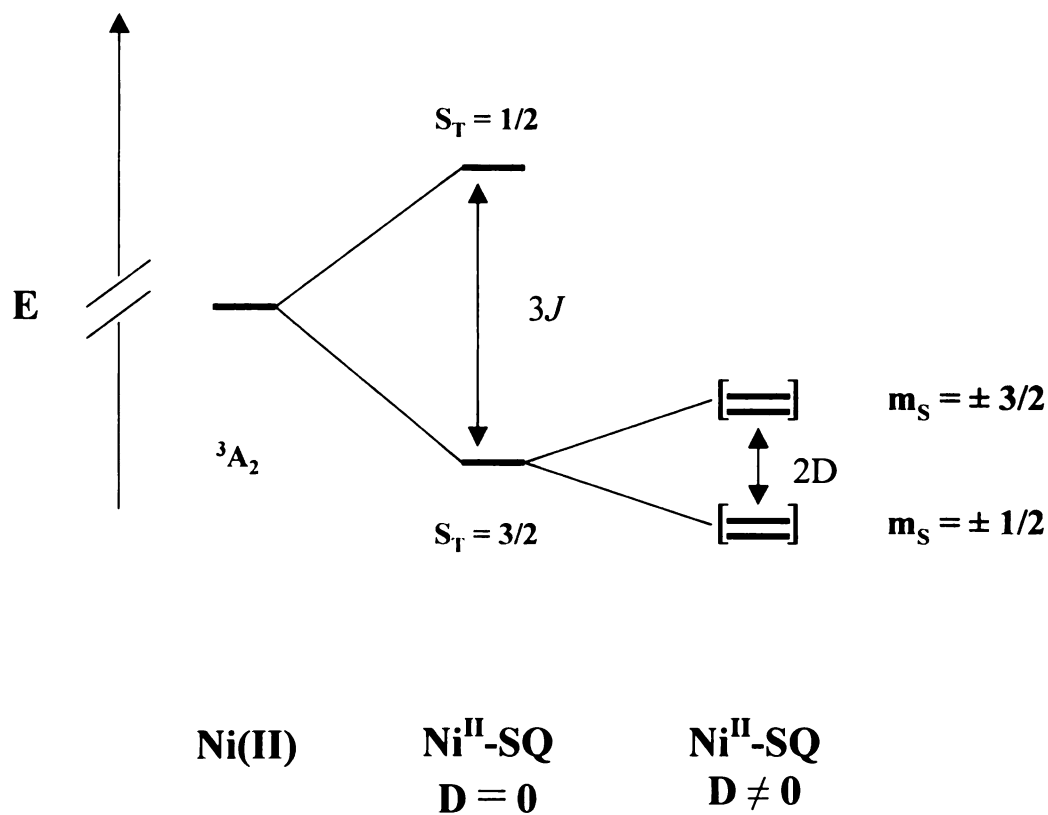


Figure 2.7. Schematic drawing of the effect of zero field splitting on the $S = 3/2$ ground state of $[\text{Ni}(\text{tren})(3,5\text{-DTBSQ})]^+$. As drawn, $D > 0$; if $D < 0$, then the $\pm 3/2$ levels would be lower in energy.

2.3.5. Electronic Absorption Spectra

The absorption spectra of non-exchange coupled six coordinate nickel(II) complexes are known to exhibit three spin allowed transitions to the 3T_2 , 3T_1 and 3T_1 levels. These occur in the range 7000 - 13,000, 11,000 - 20,000, and 19,000 - 27,000 cm^{-1} regions, respectively. In addition, a spin forbidden band to 1E_g is also observed at approximately 15,000 cm^{-1} (~ 670 nm). As seen in Figure 2.2, the transition from low-lying doublet state to the next excited state in the exchange coupled Ni(II)-SQ complex is expected to be a few hundred cm^{-1} different in energy than $^1E_g \leftarrow ^3A_2$. Therefore, we would expect the transition from the low-lying doublet excited state to the next doublet excited state ($^2B_1 \leftarrow ^2A_2$) to occur around the same region in the case of the exchange-coupled Ni(II)-semiquinone complex.

The room-temperature electronic absorption spectrum of a dichloromethane solution of $[\text{Ni}(\text{tren})(3,5\text{-DTBSQ})](\text{PF}_6)$ (Figure 2.8) shows bands at 43500 ($\epsilon = 8200 \text{ M}^{-1}\text{cm}^{-1}$), 31700 ($\epsilon = 9100 \text{ M}^{-1}\text{cm}^{-1}$), and 22700 cm^{-1} ($\epsilon = 1000 \text{ M}^{-1}\text{cm}^{-1}$) with a notable shoulder at 28200 cm^{-1} . No transitions assignable to d-d states are observed.²⁰ This spectrum is similar to that reported by Benelli et al. for $[\text{Ni}(\text{CTH})(3,5\text{-DTBSQ})]^+$.³ The similarity of this spectrum to that reported for $[\text{Zn}(\text{S,S-CTH})(3,5\text{-DTBSQ})](\text{PF}_6)$ ⁴ and the free 3,5-DTBSQ²¹ ligand indicates that these bands are likely due to internal ligand transitions involving the 3,5-DTBSQ ligand.

The magnetic data obtained for $[\text{Ni}(\text{tren})(3,5\text{-DTBSQ})](\text{PF}_6)$ shows evidence for temperature dependence in the magnetic moment. This led us to pursue variable-temperature absorption studies in hope of observing a thermochromic response. The

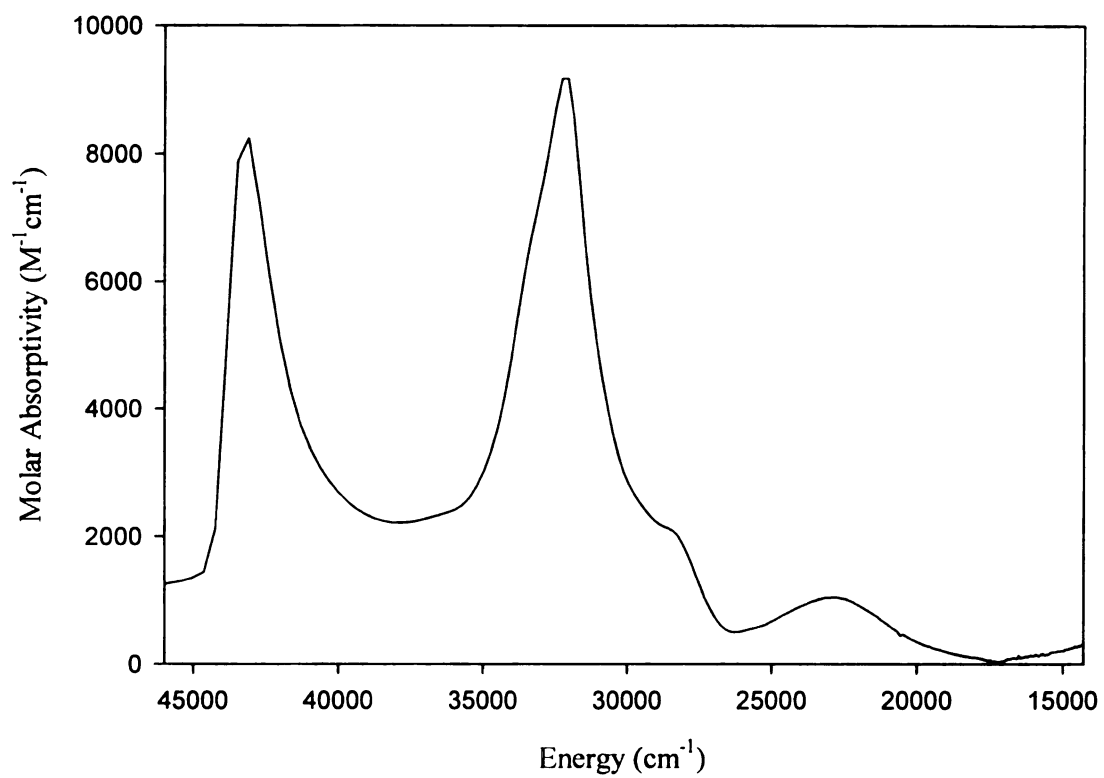


Figure 2.8. Room-temperature absorption spectrum of $[\text{Ni}(\text{tren})(3,5\text{-DTBSQ})](\text{PF}_6)$ measured in dichloromethane.

variable-temperature absorption spectra were all measured in dimethylformamide. An initial absorption spectrum was obtained at room temperature (~ 298 K) followed by acquisition of multiple absorption spectra at higher temperatures. The selected spectra are depicted below in Figure 2.9. Due to the limitations of the apparatus, we were unable to reach temperatures greater than 370 K. At the temperatures that we were able to access, the spectra showed no clear evidence of the expected absorption at ~ 670 nm.

Our inability to observe the expected thermochromic behavior can be attributed to the following. The transitions ${}^2A_2 \leftarrow {}^2A_2$ and ${}^2B_1 \leftarrow {}^2A_2$ are expected to have extinction coefficients of approximately $10^2 \text{ M}^{-1}\text{cm}^{-1}$ (based on the fact that this transition is a d-d based transition which is exchange enhanced). As seen in Figure 2.9, the extinction coefficient of the band in the region is roughly $400 \text{ M}^{-1}\text{cm}^{-1}$. Therefore, the expected band (${}^2A_2 \leftarrow {}^2A_2$ and ${}^2B_1 \leftarrow {}^2A_2$) may be obscured by this ligand-based absorption feature. This problem is likely compounded by the fact that the coupling between the Ni(II) and 3,5-DTBSQ is on the order of 150 cm^{-1} . At 320 K, this will likely lead to a ~11 % population of the 2A_2 state, further attenuating the observed intensity of the expected absorption.

2.4 Concluding Comments

This study documents the synthetic, structural, electronic, and optical properties of the pseudooctahedral $[\text{Ni}(\text{tren})(3,5\text{-DTBSQ})](\text{PF}_6)$ complex. Our goal was to utilize

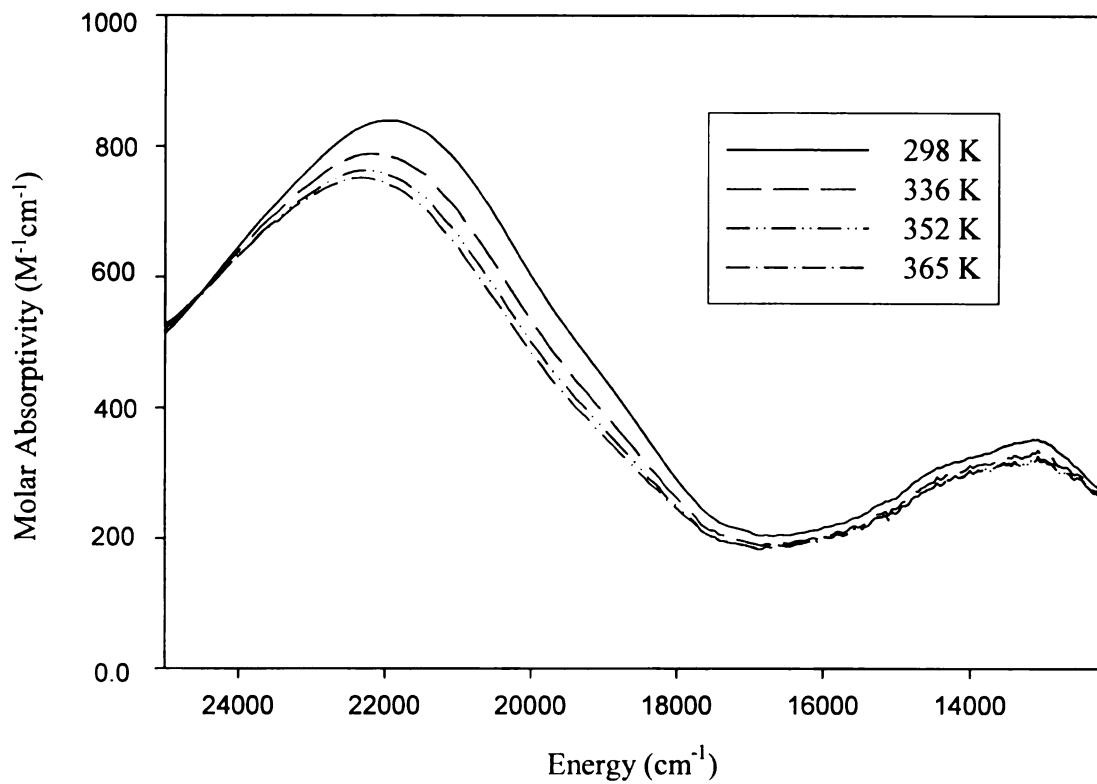


Figure 2.9. Variable-temperature electronic absorption spectra of $[\text{Ni}(\text{tren})(3,5\text{-DTBSQ})](\text{PF}_6)$ in dimethylformamide solution.

this metal-semiquinone dyad to produce a thermochromic compound. Magnetic susceptibility data confirm the expected presence of a strong ferromagnetic exchange interaction between the metal and semiquinone radical anion. The data also exhibited temperature dependence in the effective magnetic moment, however, variable-temperature absorption spectroscopy failed to show clear evidence of the expected transition from the lowest-lying doublet excited state. It was suggested that the exchange interaction might be too large, resulting in too great an energy separation between the ground state and the lowest-lying doublet excited state from which the new transition(s) is expected. One possibility to circumvent this is to employ a different semiquinone ligand which will couple more weakly to the Ni(II) center. This notion is explored in the next two chapters.

2.5 References and Notes

- (1) Benelli, C.; Dei, A.; Gatteschi, D.; Güdel, H. U.; Pardi, L. *Inorg. Chem.* **1989**, *28*, 3089.
- (2) Wheeler, D. E.; McCusker, J. K. *Inorg. Chem.* **1998**, *37*, 2296.
- (3) Benelli, C.; Dei, A.; Gatteschi, D.; Pardi, L. *Inorg. Chem.* **1988**, *27*, 2831.
- (4) Benelli, C.; Dei, A.; Gatteschi, D.; Pardi, L. *Inorg. Chem.* **1989**, *28*, 1476.
- (5) Wheeler, D. E.; Rodriguez, J. H.; McCusker, J. K. *J. Phys. Chem. A* **1999**, *103*, 4101.
- (6) Pilar, J. *J. Phys. Chem.* **1970**, *74*, 4029.
- (7) Kuwata, K.; Shimizu, Y. *Bull. Chem. Soc. Jpn.* **1969**, *42*, 864.
- (8) Rodriguez, J. H.; Wheeler, D. E.; McCusker, J. K. *J. Am. Chem. Soc.* **1998**, *120*, 12051.
- (9) Perkins, C. M. In; University of Washington, 1980.
- (10) XPREP; 5.03 ed.; Siemens Industrial Automation, Inc.: Madison, 1995.
- (11) Barrett, W. C.; Johnson, H. W.; Sawyer, D. T. *Anal. Chem.* **1984**, *56*, 1890.
- (12) Brown, D. B.; Crawford, V. H.; Hall, J. W.; Hatfield, W. E. *J. Phys. Chem.* **1977**, *81*, 1303.
- (13) Boudreaux, E. A.; Mulay, L. N. *Theory and Applications of Molecular Paramagnetism*; John Wiley and Sons: New York, 1976.
- (14) Pierpont, C. G.; Lange, C. W. *Prog. Inorg. Chem.* **1994**, *41*, 331.
- (15) Nag, K.; Chakravorty, A. *Coord. Chem. Rev.* **1980**, *33*, 87.
- (16) Olson, D. C.; Vasilevskij, J. *Inorg. Chem.* **1969**, *8*, 1611.

- (17) Lehman, M. W.; Evans, D. H. *J. Electroanal. Chem.* **2001**, *500*, 12.
- (18) Kambe, K. *J. Phys. Soc. Jpn.* **1950**, *48*, 5.
- (19) The temperature-independent paramagnetism (TIP) value for this complex was assumed to be $250 \times 10^6 \text{ cm}^3/\text{mol}$
- (20) The d-d transition (${}^1E \leftarrow {}^3A_2$) is known to occur at $\sim 650 \text{ nm}$ for non-exchange coupled octahedral complexes.
- (21) Stallings, M. D.; Morrison, M. M.; Sawyer, D. T. *Inorg. Chem.* **1981**, *20*, 2655.

CHAPTER THREE

Synthesis and Magnetic Properties of Cr(3,5-DTBSQ)₃ and Cr(PhenSQ)₃

3.1 Introduction

The synthesis and characterization of the complex, [Ni(tren)(3,5-DTBSQ)](PF₆) was explored in the previous chapter. The function of that complex was to study thermochromism, which is expected to arise due to exchange coupling between the Ni(II) and semiquinone ligand. The results obtained from variable-temperature absorption studies of the complex, [Ni(tren)(3,5-DTBSQ)](PF₆), failed to show clear evidence of thermochromic behavior. It was suggested that the energy gap ($\Delta E = 3J$) between the ground state and the low-lying excited state might be too large to produce enough thermal population of the doublet excited state. In order to decrease this gap, a new quinone must be chosen which couples more weakly to the Ni(II).

A large number of complexes containing multiple radical semiquinone ligands chelated to paramagnetic metal ions have been studied. Specifically, the preparations of Cr(3,5-DTBSQ)₃¹⁻⁸ and Cr(PhenSQ)₃^{3,8-11} (PhenSQ = phenanthrenesemiquinone) have been reported along with partial characterization of their magnetic properties. These studies indicate the presence of strong antiferromagnetic coupling between the metal and radical semiquinone ligands in both molecules. In this chapter, the magnetic properties of Cr(3,5-DTBSQ)₃ and Cr(PhenSQ)₃ will be examined in more detail. Specifically, the magnetic susceptibility data will be acquired and fit to the Van Vleck equation in order to

extract the coupling constant between Cr-SQ. Values obtained for J will give us insight into the possible difference in coupling between PhenSQ and 3,5-DTBSQ given a common environment (i.e., coupling to Cr(III)) and provide an indication as to whether PhenSQ might be a more suitable ligand to achieve thermochromism in a Ni(II) system.

3.2 Experimental Section

3.2.1. General

All reagents and materials were obtained from commercial sources and were used as received. Solvents were purchased from either Aldrich Chemical Co. or Strem. Elemental analyses were obtained through the Analytical Facilities of Michigan State University.

3.2.2 Synthesis of Cr(3,5-DTBSQ)₃

Preparative procedures for this complex have previously been reported.^{3,12} The dark violet crystals were washed with absolute ethanol (3 x 25 mL) and recrystallized from 1:1 toluene/ethanol. Anal. Calcd. CrC₄₂H₆₀O₆: C, 70.76; H, 8.48; N, 0.00. Found: C, 71.36; H, 8.62; N, 0.14.

3.2.3 Synthesis of Cr(PhenSQ)₃

The synthesis of this compound has been previously reported.^{3,9,10,12} The dark violet crystals that precipitated upon cooling were collected and washed with toluene (3 x 25 mL) followed by ethanol (3 x 25 mL). Anal. Calcd. CrC₄₂H₂₄O₆: C, 74.55; H, 3.58; N, 0.00. Found: C, 75.50; H, 3.57; N, 0.10.

3.2.4 Variable-Temperature Magnetic Susceptibility

Magnetic susceptibility data were collected as described for [Ni(tren)(3,5-DTBSQ)](PF₆) in Chapter 2. Data were collected at a magnetic field strength of 2.5 T and corrected for diamagnetism using Pascal's constants.¹³ The data were fit to Equations 1.7 using a program of local origin to obtain a value for the exchange coupling constant, *J*.

3.3 Results and Discussion

3.3.1 Magnetism of Cr(3,5-DTBSQ)₃

Variable-temperature magnetic susceptibility data for Cr(3,5-DTBSQ)₃ is illustrated in Figure 3.1 as a plot of the effective magnetic moment versus temperature. At 380 K, the effective magnetic moment is 1.13 μ_B and decreases to a value of 0.17 μ_B at 5 K. This is significantly lower than the spin-only value for a system comprised of non-

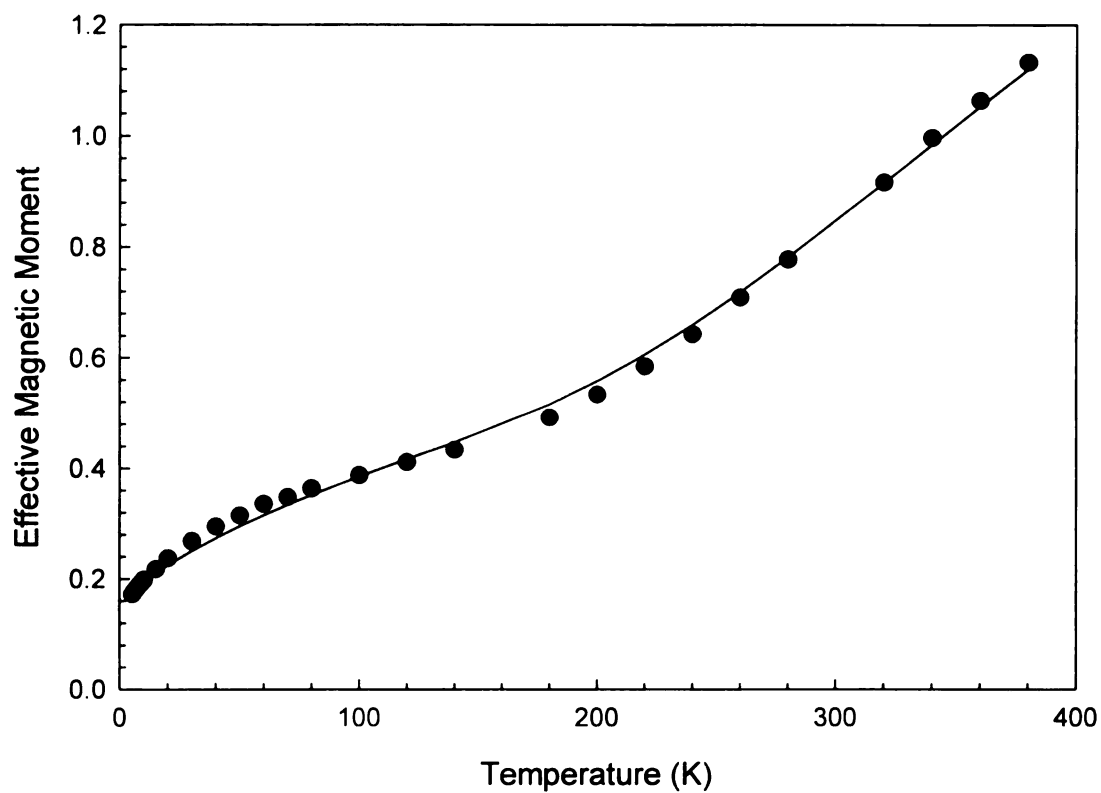


Figure 3.1. Plot of effective magnetic moment versus temperature for $\text{Cr}(3,5\text{-DTBSQ})_3$ (circles). The solid line represents the fit to a theoretical model; $g = 2.00$, $\text{TIP} = 150 \times 10^6 \text{ cm}^3/\text{mol}$, and $J = -440 \text{ cm}^{-1}$.

exchange coupled Cr(III) and three radical semiquinones, implying that the coupling between the metal and the ligands is antiferromagnetic in nature.

The exchange interactions within this molecule can be described by a simple Heisenberg exchange Hamiltonian shown below in Equation 3.1,

$$\mathbf{H} = -2 \sum_i \sum_j J_{ij} \mathbf{S}_i \cdot \mathbf{S}_j \quad (3.1)$$

where the terms are those previously described in Chapters 1 and 2.

In the case of Cr(3,5-DTBSQ)₃, or Cr(SQ)₃ in general, there are two exchange interactions present: direct exchange between the metal and each semiquinone ligand, as well as superexchange between the semiquinone ligands. The complete Hamiltonian accounting for all pairwise interactions can be written as

$$\begin{aligned} \mathbf{H} = & -2J [\mathbf{S}_{\text{Cr}} \cdot \mathbf{S}_{\text{SQ1}} + \mathbf{S}_{\text{Cr}} \cdot \mathbf{S}_{\text{SQ2}} + \mathbf{S}_{\text{Cr}} \cdot \mathbf{S}_{\text{SQ3}}] \\ & -2J' [\mathbf{S}_{\text{SQ1}} \cdot \mathbf{S}_{\text{SQ2}} + \mathbf{S}_{\text{SQ2}} \cdot \mathbf{S}_{\text{SQ3}} + \mathbf{S}_{\text{SQ1}} \cdot \mathbf{S}_{\text{SQ3}}] \end{aligned} \quad (3.2)$$

where due to the D₃ symmetry of the molecule, $J_{\text{Cr-SQ1}} = J_{\text{Cr-SQ2}} = J_{\text{Cr-SQ3}} = J$ and $J_{\text{SQ1-SQ2}} = J_{\text{SQ2-SQ3}} = J_{\text{SQ1-SQ3}} = J'$. The magnitude of direct exchange is expected to be much larger than that of superexchange.¹⁴ For example, the exchange constant corresponding to superexchange between the 3,5-DTBSQ ligands in the compound Ga(3,5-DTBSQ)₃ was determined to be 7.8 cm⁻¹ compared to several hundred cm⁻¹ typical of metal-semiquinone coupling.¹⁵ Therefore, as first approximation, the only exchange parameter that will be considered is the Cr-SQ interaction. The spin Hamiltonian now becomes

$$\mathbf{H} = -2J [\mathbf{S}_{Cr} \cdot \mathbf{S}_{SQ1} + \mathbf{S}_{Cr} \cdot \mathbf{S}_{SQ2} + \mathbf{S}_{Cr} \cdot \mathbf{S}_{SQ3}] \quad (3.3)$$

Prior to employing the Kambe approximation, we define a general spin operator, \mathbf{S}_A (Equation 3.4).

$$\mathbf{S}_A = \mathbf{S}_{SQ1} + \mathbf{S}_{SQ2} + \mathbf{S}_{SQ3} \quad (3.4)$$

Squaring Equation 3.4 affords Equation 3.5.

$$\mathbf{S}_A^2 = \mathbf{S}_{SQ1}^2 + \mathbf{S}_{SQ2}^2 + \mathbf{S}_{SQ3}^2 + 2\mathbf{S}_{SQ1} \cdot \mathbf{S}_{SQ2} + 2\mathbf{S}_{SQ2} \cdot \mathbf{S}_{SQ3} + 2\mathbf{S}_{SQ1} \cdot \mathbf{S}_{SQ3} \quad (3.5)$$

In addition, the product $\mathbf{S}_{Cr} \cdot \mathbf{S}_A$ is given in Equation 3.6.

$$\mathbf{S}_{Cr} \cdot \mathbf{S}_A = \mathbf{S}_{Cr} \cdot \mathbf{S}_{SQ1} + \mathbf{S}_{Cr} \cdot \mathbf{S}_{SQ2} + \mathbf{S}_{Cr} \cdot \mathbf{S}_{SQ3} \quad (3.6)$$

Therefore, by applying the Kambe approximation¹⁶ and using the fact, $\mathbf{S}_T = \mathbf{S}_{Cr} + \mathbf{S}_{SQ1} + \mathbf{S}_{SQ2} + \mathbf{S}_{SQ3}$ (or $\mathbf{S}_T = \mathbf{S}_{Cr} + \mathbf{S}_A$), the square of total spin operator can be written as

$$\mathbf{S}_T^2 = \mathbf{S}_{Cr}^2 + \mathbf{S}_A^2 + 2\mathbf{S}_{Cr} \cdot \mathbf{S}_A \quad (3.7)$$

or simply

$$\mathbf{S}_{Cr} \cdot \mathbf{S}_A = 1/2(\mathbf{S}_T^2 - \mathbf{S}_{Cr}^2 - \mathbf{S}_A^2) \quad (3.8)$$

Substituting Equation 3.8 into Equation 3.6 and 3.3 affords Equation 3.9.

$$\mathbf{H} = -J [S_T^2 - S_A^2 - S_{Cr}^2] \quad (3.9)$$

From this equation, the eigenvalue expression can be generated, Equation 3.10, and the eigenvalues can be obtained.

$$E(S) = -J [S_T(S_T+1) - S_A(S_A+1) - S_{Cr}(S_{Cr}+1)] \quad (3.10)$$

The resulting energy levels for Cr(3,5-DTBSQ)₃, or any analogous Cr(SQ)₃ complex, are depicted in Figure 3.2. The magnetic properties of Cr(SQ)₃ as a function of temperature reflect a Boltzman distribution over the thermally accessible spin states shown in Figure 3.2. The general expression that describes magnetic susceptibility is given by Equation 1.7. The variable temperature magnetic susceptibility data were fit to this expression using the eigenvalues of Equation 3.10. The solid line in Figure 3.1 corresponds to the best fit with parameters of $g = 2.00$ and $J = -440 \text{ cm}^{-1}$; temperature independent paramagnetism (TIP) was fixed at $150 \times 10^{-6} \text{ cm}^3/\text{mol}$.

3.3.2 Magnetism of Cr(PhenSQ)₃ and Comparison with Cr(3,5-DTBSQ)₃

The variable-temperature magnetic susceptibility data obtained by other workers for Cr(PhenSQ)₃ displayed residual paramagnetism at higher temperatures.^{8,9} At 286 K, Cr(PhenSQ)₃ was found to have a magnetic moment value of $1.15 \mu_B$, which decreases to

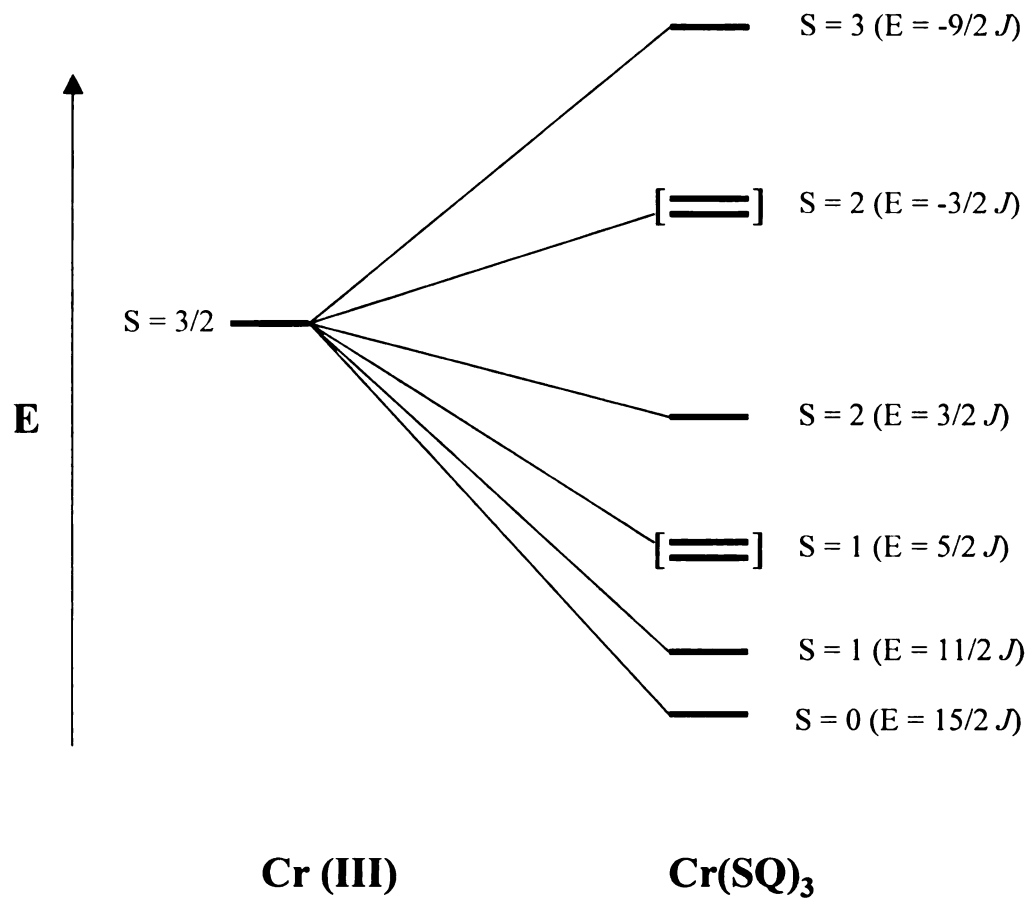


Figure 3.2 Energy levels for $\text{Cr}(\text{SQ})_3$ complexes resulting from intramolecular antiferromagnetic exchange between the unpaired electrons of the *o*-semiquinone ligands and the $\text{Cr}(\text{III})$ ion.

0.30 μ_B at 4.2K.⁸ This is consistent with the formulation of an antiferromagnetically coupled Cr(PhenSQ)₃ system. The exchange parameter for this compound was determined by Lynch et al. to be -350 cm^{-1} .¹¹

The variable-temperature magnetic susceptibility data we obtained for this complex are summarized in Figure 3.3 as a plot of the effective magnetic moment versus temperature in the range 5 – 380 K. An attempt to fit the magnetic susceptibility data to Equations 1.7 was hindered by the inability to accurately compensate for background contributions. We can, however, infer that the coupling between Cr(III)-PhenSQ is weaker than Cr(III)-3,5-DTBSQ from the data due to the fact that the effective moment of the former complex is greater than that of the latter complex (Figure 3.3).

The coupling constant obtained for Cr(3,5-DTBSQ)₃ in this study clearly indicates that 3,5-DTBSQ couples more strongly than PhenSQ to Cr(III). Although the strength of exchange interactions are affected by numerous factors, including orbital energetics, it is nonetheless reasonable to expect that the coupling between PhenSQ and a given metal ion should be smaller than that observed between 3,5-DTBSQ and that same metal, given the same geometric environment. The phenanthrenesemiquinone version of [Ni(tren)(3,5-DTBSQ)]⁺ is therefore expected to exhibit a smaller coupling constant and a greater likelihood of exhibiting thermochromic behavior.

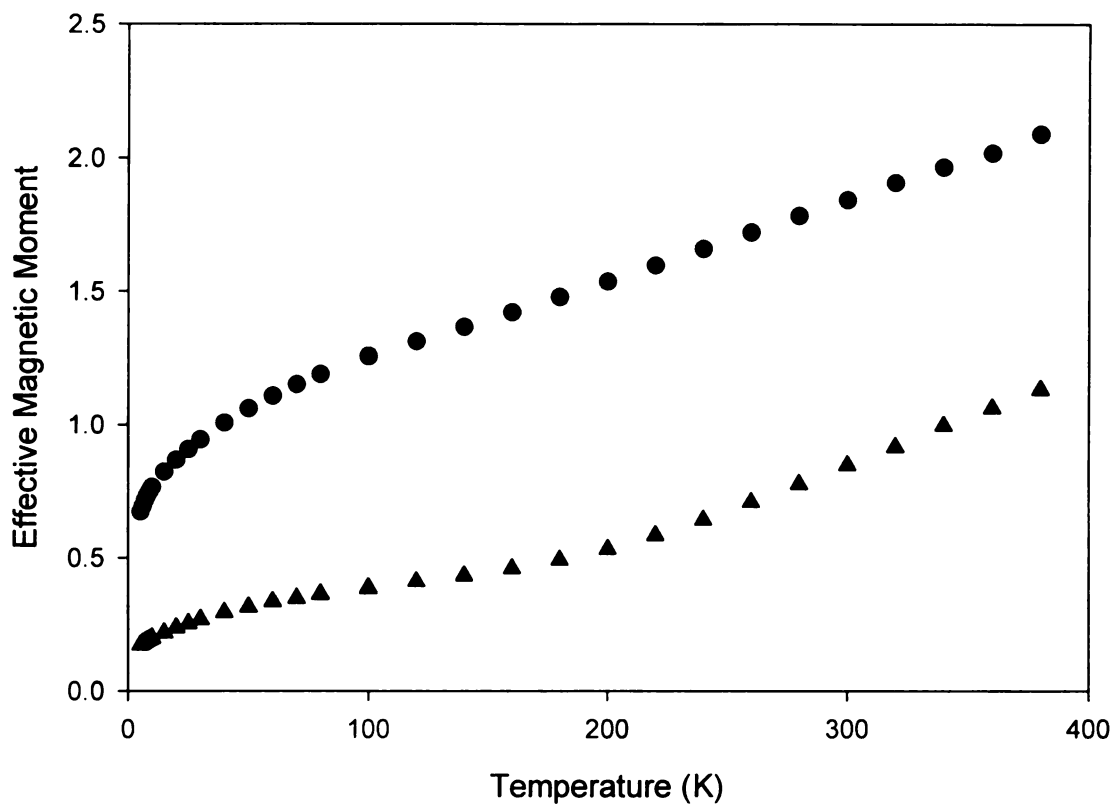


Figure 3.3 Plots of effective magnetic moment versus temperature for $\text{Cr}(\text{PhenSQ})_3$ (circles) and $\text{Cr}(3,5\text{-DTBSQ})_3$ (triangles).

3.4 References and Notes

- (1) Abakumov, G. A. *Izv. Akad. Nauk, Ser. Khim.* **1977**, 7, 1642.
- (2) Danek, M.; Vicek, A., Jr. *Proc. Conf. Coord. Chem.* **1989**
- (3) Downs, H. H.; Buchanan, R. M.; Pierpont, C. G. *Inorg. Chem.* **1979**, 18, 1736.
- (4) Glushakova, V. N.; Skorodumova, N. A.; Mitin, A. V.; Nevodchikov, V. I.;
Abukumova, L. G.; Lovanov, A. V. *Izv. Akad. Nauk, Ser. Khim.* **1994**, 2, 327.
- (5) Lovanov, A. V.; Abakumov, G. A.; Razuvaev, G. A. *Dokl. Akad. Nauk SSR* **1977**,
235, 824.
- (6) Sofen, S. R.; Ware, D. C.; Cooper, S. R.; Raymond, K. N. *Inorg. Chem.* **1979**, 18,
234.
- (7) Vclek, A., Jr. *Inorg. Chem.* **1986**, 25, 522.
- (8) Buchanan, R. M.; Downs, H. H.; Shorthill, W. B.; Pierpont, C. G.; Kessel, S. L.;
Hendrickson, D. N. *J. Am. Chem. Soc.* **1978**, 100, 7894.
- (9) Buchanan, R. M.; Downs, H. H.; Shorthill, W. B.; Pierpont, C. G.; Kessel, S. L.;
Hendrickson, D. N. *J. Am. Chem. Soc.* **1978**, 100, 4318.
- (10) Vlckova, B.; Stepanek, J. *Proc. Conf. Coord. Chem.* **1987**, 11, 463.
- (11) Lynch, M. W.; Buchanan, R. M.; Pierpont, C. G.; Hendrickson, D. N. *Inorg.*
Chem. **1981**, 20, 1038.
- (12) Brown, D. G.; Johnson, L. Z. *Naturforsch* **1979**, 34b, 712.
- (13) Boudreaux, E. A.; Mulay, L. N. *Theory and Applications of Molecular*
Paramagnetism; John Wiley and Sons: New York, 1976.
- (14) Pierpont, C. G.; Attia, A. S. *Collect. Czech. Chem. Commun.* **2001**, 66, 33.

- (15) Adams, D. M.; Rheingold, A. L.; Dei, A.; Hendrickson, D. N. *Angew. Chem., Int. Ed. Engl.* **1994**, *32*, 391.
- (16) Kambe, K. *J. Phys. Soc. Jpn.* **1950**, *48*, 5.

CHAPTER FOUR

Density Functional Theory Analysis of the Electronic Structures of Phenanthrenequinone and Phenanthrenesemiquinone

4.1 Introduction

Quinones are commonly exploited for their innate redox properties.¹ Upon reduction to the semiquinone redox state, the diamagnetic quinone ($S = 0$) becomes paramagnetic ($S = 1/2$). Further reduction yields the diamagnetic ($S = 0$) catecholate form. All three redox states are known to be stable; however, the quinone redox state is not as useful for coordination chemistry due to its poor binding affinity to a metal center. Metal-semiquinone complexes have been utilized as models by many inorganic chemists in the study of simple intramolecular exchange coupling. For example, several complexes of metals ranging from chromium, copper, zinc, to nickel among others have been studied.²⁻¹³ Common semiquinone ligands include tetrachlorobenzosemiquinone (TCSQ), 3,5-di-*tert*-butylsemiquinone (3,5-DTBSQ), 3,6-di-*tert*-butylsemiquinone (3,6-DTBSQ), and phenanthrenesemiquinone (PhenSQ). Our interest in these systems stems from the opportunity they afford for effectively turning on (SQ) or off (Cat) exchange coupling by converting from one redox state to the other.²

Theoretical studies have also been performed on quinones and metal-quinone complexes.¹⁴⁻¹⁶ Fenske-Hall calculations, which is a nonempirical molecular orbital

method, have been reported on the free quinone ligand for inclusion in a study of the bonding present in metal-quinone complexes.¹⁴ Bianchini, et al.¹⁷, performed extended Hückel and fragment molecular orbital calculations on the unsubstituted quinone for a study involving Co-quinone complexes. This study presented qualitative results that were used to describe magnetic properties as well as a mechanism for electron transfer in these compounds. In addition, density functional theory (DFT) has been applied to the free semiquinone ligand, which proved useful in the analysis of the electronic structure variations across the redox series of the 3,6-di-*tert*-butylbenzoquinone and 3,5-di-*tert*-butylbenzoquinone.¹⁸ The results found in this study detailed the molecular orbital compositions, overall relative ordering of the molecular orbitals, localization of the NPA charge densities, and localization of the unpaired spin densities. The calculations carried out by Rodriguez, et al. detailed the mechanism of exchange between chromium(III) and a single semiquinone ligand.¹⁶

The results of the previous chapter suggest that phenanthrenesemiquinone might afford a smaller exchange constant when bound to Ni(II) than does 3,5-DTBSQ. By analogy to previous work from our lab,^{16,18} this chapter describes a computational study of both phenanthrenequinone and phenanthrenesemiquinone in order to gain insight into their electronic structures. The primary goals of this study will be to explore the spatial distribution of the molecular orbitals and the relative ordering of energy levels of the molecular orbitals upon reduction from the quinone to the semiquinone redox state. The catechol redox state will not be considered.

4.2 Computational Methods

4.2.1 General Methods

The self-consistent field (SCF) density functional calculations were performed using the Gaussian 98 program.¹⁹ The two different hybrid functionals used were the BLYP functional and the B3LYP functional. The BLYP functional combines the gradient-corrected Becke (B) exchange with the nonlocal correlation functional of Lee, Yang, and Parr (LYP).²⁰ The hybrid B3LYP functional combines the three parameter exchange of Becke²¹⁻²³ with the LYP correlation functional. All calculations were done using tight convergence criteria.²⁴ The atomic charge analyses were performed using the natural population analysis (NPA) framework developed by Weinhold et al.²⁵⁻²⁷

4.2.2. Geometry Optimizations

The optimization was carried out in three steps. First, the geometry was optimized using restricted Hartree-Fock (RHF) methods for phenanthrenequinone (PhenQ) and restricted open shell Hartree-Fock (ROHF) for phenanthrenesemiquinone (PhenSQ). An STO-3G** basis set was used in each case. No geometrical constraints were imposed on the molecule. The starting geometry used for the first optimization was obtained from an X-ray structure that has been reported for phenanthrenequinone.²⁸ There were several forms of the crystal reported²⁸ but the exact form chosen for this calculation was the α -form of the PhenQ crystal. The labeling scheme and coordinate system used for both

molecules is shown in Figure 4.1. After the first optimization, a second optimization was performed at the BLYP/3-21G** level using restricted density functional theory (RDFT) and restricted open-shell density functional theory (RODFT) for the quinone and semiquinone forms, respectively. The final optimization was performed at the B3LYP/6-31G* level using either RDFT or RODFT. The optimized geometry obtained at this level was then used in subsequent single point calculations.

4.2.3. Single Point Calculation

The calculations carried out for the singlet PhenQ incorporated the B3LYP functional and a 6-311G** basis set. The molecular charge was designated to be zero. The calculations performed for the doublet PhenSQ involved a similar functional and basis set, however, the molecular charge in this case was assumed to be -1 . Separate geometry optimizations and single-point calculations were carried out on PhenQ assuming singlet and triplet configurations. The optimized structure obtained for the singlet configuration produced a lower total SCF energy relative to the triplet, confirming that the ground state of phenanthrenequinone is a singlet. Similar calculations were performed for the semiquinone, assuming doublet and quartet configurations: the total SCF energy of the doublet was significantly lower than the quartet. The total SCF energies obtained for both the quinone and the semiquinone molecules are given in Table 4.1.

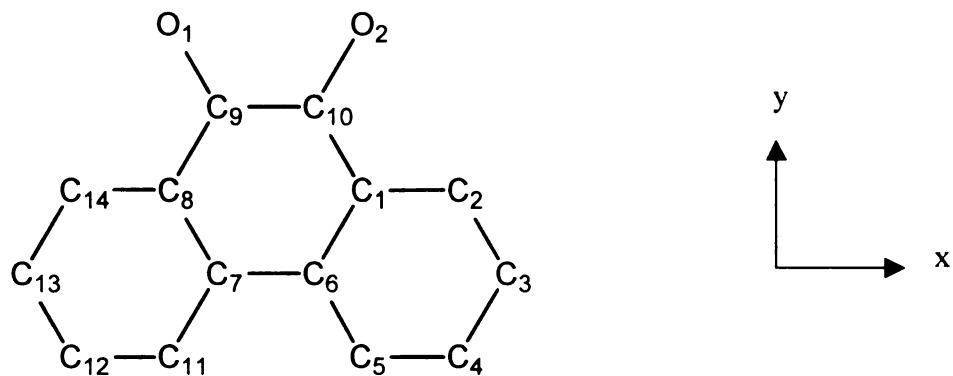


Figure 4.1. The labeling scheme and coordinate system used for phenanthrenequinone and phenanthrenesemiquinone. The peripheral carbons are defined as C2, C3, C4, C5, C11, C12, C13, and C14.

Table 4.1. Total Self-Consistent Field Energies (Hartree) Obtained at the B3LYP/6-311G** Level Using the Optimized Geometries of PhenQ and PhenSQ

Molecule	2S + 1	Energy
Phenanthrenequinone	1	-688.924912
	3	-688.856575
Phenanthrenesemiquinone	2	-688.987181
	4	-688.865211

4.3 Results and Discussion

4.3.1. Optimized Geometries of PhenQ and PhenSQ

The redox states of phenanthrenequinone are depicted in Figure 4.2. The structural parameters obtained from the optimization of PhenQ and PhenSQ are listed in Table 4.2. The bond lengths obtained for PhenQ are reasonably similar to those reported for the X-ray crystal structure.²⁸ The trends observed in the optimized geometry of PhenQ are similar to those found for other quinones. The longest bond in the molecule is between C9-C10, which is 1.545 Å. The bonds between C1-C6 and C7-C8 exhibit lengths of 1.416 Å which are the shortest bond lengths within the ring. These results reflect the bonding characteristics expected for quinones where the shortest bonds in the optimized structure are designated in the literature²⁹ as those having the most double bond character within the ring. The bonds between C9-O1 and C10-O2 exhibit distances of 1.219 Å, typical of a C=O bond.

Reduction of the quinone to the semiquinone redox state is accompanied by appreciable geometric changes. In general, one observes a shortening of the single bonds and elongation of the double bonds of the quinone upon addition of an electron. For example, the bond between C9-C10 shortens by approximately 0.06 Å and the bonds between C1-C6 and C7-C8 lengthen by approximately 0.01 Å. Another noteworthy change is the lengthening of the carbon-oxygen bonds by approximately 0.04 Å. This is reasonable considering that a one-electron reduction eliminates one C-O double bond to yield a double bond which is delocalized over two carbon-oxygen pairs. These structural

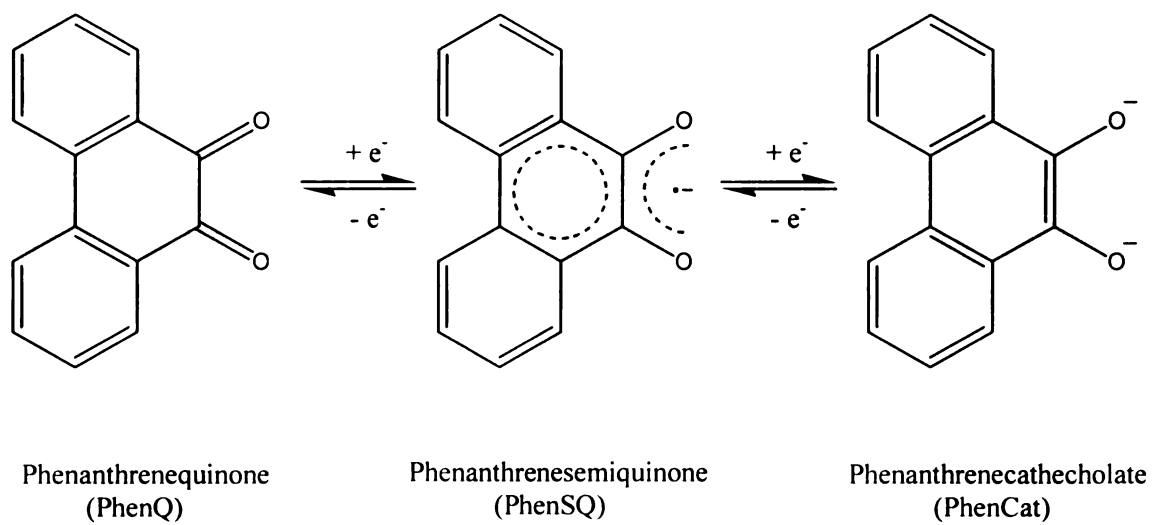


Figure 4.2. The redox states of phenanthrenequinone.

Table 4.2. Selected Bond Lengths (Å) for Phenanthrenequinone (PhenQ) and Phenanthrenesemiquinone (PhenSQ) Obtained from Experiment and Self-Consistent Field (SCF) Geometry Optimizations at the B3LYP/6-31G* Level

Bond	PhenQ (exp) ^a	PhenQ (calc)	PhenSQ (calc)
C(1)-C(2)	1.39	1.402	1.413
C(2)-C(3)	1.34	1.389	1.383
C(3)-C(4)	1.38	1.398	1.408
C(4)-C(5)	1.38	1.393	1.387
C(5)-C(6)	1.39	1.405	1.413
C(1)-C(6)	1.41	1.416	1.427
C(6)-C(7)	1.48	1.485	1.462
C(7)-C(8)	1.41	1.416	1.427
C(8)-C(9)	1.47	1.484	1.477
C(9)-C(10)	1.51	1.545	1.481
C(1)-C(10)	1.47	1.484	1.477
C(7)-C(11)	1.39	1.405	1.413
C(11)-C(12)	1.38	1.393	1.387
C(12)-C(13)	1.38	1.398	1.408
C(13)-C(14)	1.34	1.389	1.383
C(8)-C(14)	1.39	1.402	1.413
C(9)-O(1)	1.25	1.219	1.255
C(10)-O(2)	1.25	1.219	1.255

^a Matsuzaki, S.Y., Gotoh, M., Kuboyama, A. *Mol. Cryst. Liq. Cryst.*, **1987**, 142, 127

changes are also in accord with qualitative expectations based on the character of the molecular orbitals involved (vide infra).

4.3.2. Molecular Orbitals of Phenanthrenequinone (PhenQ)

The energies and atomic contributions of the highest occupied and lowest unoccupied molecular orbitals (MOs) 52-56 are summarized in Table 4.3. The α and β orbitals (1 e^- orbitals of differing spin) of PhenQ were found to be identical in energy and composition, as expected for this closed-shell singlet. The highest molecular orbital (HOMO) and lowest unoccupied molecular orbital (LUMO) of phenanthrenequinone are MO 54 α,β and MO 55 α,β respectively.

The occupied molecular orbitals 52 α,β are mostly comprised of orbital contribution from C1, C8, and the carbons of the peripheral rings (C2, C4, C5, C11, C12, C14). They contribute approximately 11 % each to these molecular orbitals. Figure 4.3 shows the spatial representation of MO 52 α . From this figure, it is apparent that the oxygen atoms are relatively isolated from each other, exhibiting only very weak π anti-bonding interactions. It is also apparent that much of the interaction occurs between the carbons within the peripheral rings. For example, π bonding interactions is observed in the following carbon pairs, C1-C2, C4-C5, C11-C12, and C8-C14 (Figure 4.3).

The next highest occupied molecular orbitals, 53 α,β , are composed mostly of p_x and p_y orbitals on the oxygens (ca. 32 % each). As shown in Table 4.3, additional contributions (of less than ca. 10%) are provided by C1, C8, C9, and C10. The contributions from the carbons of the peripheral rings are negligible in this case. The

Table 4.3. Energies and Percent Atomic Contributions to the Frontier Molecular Orbitals of Phenanthrenequinone (PhenQ) Obtained at the U-B3LYP/6-311G** Level

Orbital ^a	52 α,β	53 α,β	54 α,β	55 α,β	56 α,β
Type ^b	O	O	O	V	V
Energy (eV)	-7.515	-6.871	-6.853	-3.253	-1.679
% C1	11.12	8.41	7.26	3.31	1.17
% C2	11.31	1.78	3.03	4.04	10.12
% C3	0.02	0.19	15.99	1.36	13.12
% C4	11.22	0.07	1.63	5.77	0.24
% C5	10.83	0.45	8.36	0.14	15.11
% C6	0.00	0.64	11.97	4.73	8.68
% C7	0.00	0.73	11.97	4.73	8.68
% C8	11.12	8.37	7.26	3.31	1.17
% C9	0.01	5.85	0.03	12.04	1.04
% C10	0.01	5.71	0.03	12.04	1.04
% C11	10.83	0.39	8.36	0.14	15.11
% C12	11.22	0.10	1.63	5.77	0.24
% C13	0.02	0.24	15.99	1.36	13.12
% C14	11.31	1.68	3.03	4.04	10.12
% O1	5.49	32.19	1.73	18.61	0.53
% O2	5.49	32.11	1.73	18.61	0.53

^a The α and β orbitals for this molecule were found to be identical energetically and in composition. ^b V = virtual (unoccupied); O = occupied

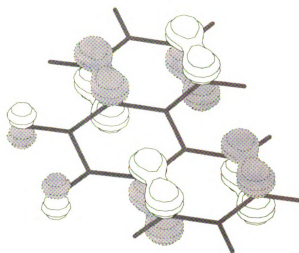


Figure 4.3. MO 52 α of phenanthrenequinone. The orbital density is localized above and below the plane of the ring.

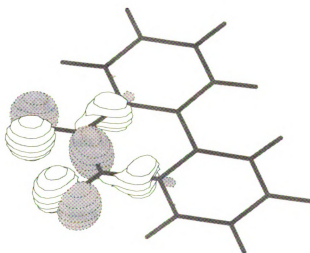


Figure 4.4. MO 53 α of phenanthrenequinone. The orbital lies in the plane of the ring.

principal interaction, as depicted in Figure 4.4, is the π -antibonding interaction occurring between the oxygen and carbon orbitals.

The HOMOs for PhenQ are MOs 54 α,β , which are depicted in Figure 4.5. They are comprised mainly of contributions from the carbons (C3, C13, C5, C11) of the peripheral rings. Also significant are the contributions from C6 and C7 (ca. 12 %). The oxygens, O1 and O2, contribute negligibly (1.73 %) to these molecular orbitals; C9 and C10 contribute less than 1 %. Table 4.3 lists the other contributions to these molecular orbitals. Interestingly, this result differs from what was found previously¹⁸ for the HOMOs of 3,6-di-*tert*-butylquinone (3,6-DTBQ). Wheeler et al. found that the HOMOs of 3,6-DTBQ were mainly composed of contributions from the oxygen atoms (18.5 % each) while the contributions from the carbons of the ring were less significant.

The quinone LUMOs (55 α,β , Figure 4.6) are composed mostly of p_z orbitals on the oxygen atoms, contributing 18.61 % each. The next major contributors are C9 and C10, (ca. 12 %). As seen in Figure 4.6, π -antibonding interactions are present between the oxygen (O1 and O2) and carbon (C9 and C10) atoms. There are also weak π -bonding interactions between C1, C8, C9, and C10.

The last molecular orbitals that will be considered for phenanthrenequinone are the degenerate MOs 56 α,β . Main contributions come from the p_z orbitals of C5 and C11 (15.11 %). Carbons 3 and 13 each contribute 13.12 % whereas C2 and C14 contribute 10.12 %. In addition, C6 and C7 contribute ca. 9 % to these molecular orbitals. The other carbons in the ring and peripheral rings contribute less than 1 %. Overall, the main interactions in these molecular orbitals are thus strong π -antibonding interactions between the carbons in the peripheral rings. This is clearly seen in Figure 4.7.

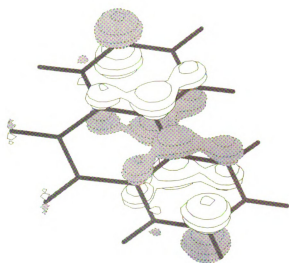


Figure 4.5. MO 54a (HOMO) of phenanthrenequinone. The orbital density lies above and below the plane of the ring.

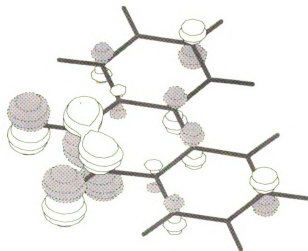


Figure 4.6. MO 55a (LUMO) of phenanthrenequinone. The orbital density lies above and below the plane of the ring.

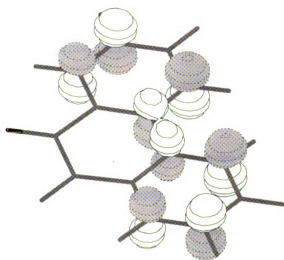


Figure 4.7. MO 56 α of phenanthrenequinone. The orbital density lies above and below the plane of the ring.

4.3.3. Molecular Orbitals of Phenanthrenesemiquinone (PhenSQ)

The next molecule examined here is PhenSQ. Table 4.4 lists the energies and composition of orbitals 52-56. For the purpose of discussion, only the similarities and differences of the orbitals of this molecule with those of phenanthrenequinone will be discussed rather than the details of every orbital.

Upon reduction, the quinone undergoes significant changes in geometry. These changes are in accord with the bonding and antibonding interactions present in the lowest unoccupied molecular orbital (LUMO) of the PhenQ which becomes occupied upon reduction. The principal interaction in the LUMO between C1-C6 and C7-C8, as depicted in Figure 4.6, is π -antibonding which contributes to the lengthening of the bond upon reduction. In contrast, the principle interaction between C9-C10 is π -bonding which results in shortening of the bond upon reduction.

Molecular orbital 55 α (HOMO) of phenanthrenesemiquinone bears a remarkable resemblance to molecular orbital 55 (LUMO) of phenanthrenequinone. Despite the fact that MO 55 is unoccupied in PhenQ and occupied in PhenSQ, its spatial distribution remains virtually unchanged. Therefore, the Aufbau principle applies in this system, where an electron placed in the LUMO of PhenQ represents, to a good approximation, the correct valence electronic structure of the one-electron reduced species. However, it is interesting to note that several of the lower energy orbital compositions of PhenQ and PhenSQ are quite different. This is in stark contrast to what was found for the ligands 3,5-DTBQ and 3,6-DTBQ,¹⁸ the spatial distributions of most of the higher energy occupied molecular orbitals remained virtually identical upon reduction of the quinone to

Table 4.4. Energies and Percent Atomic Contributions to the Frontier Molecular Orbitals of Phenanthrenesemiquinone Obtained at the U-B3LYP/6-311G** Level

Orbital	52 α	52 β	53 α	53 β	54 α	54 β	55 α	55 β	56 α	56 β
Type ^a	O	O	O	O	O	O	O	V	V	V
Energy (eV)	-2.884	-2.697	-2.705	-2.455	-2.033	-1.859	-0.216	1.542	2.305	2.386
% C1	2.41	2.25	10.95	12.06	8.06	7.76	3.43	8.02	53.58	0.20
% C2	0.58	1.00	0.65	0.09	1.12	1.62	3.51	1.99	15.27	13.33
% C3	0.07	0.17	14.06	10.14	0.06	0.08	1.48	3.62	0.04	10.49
% C4	0.04	0.08	2.83	4.87	0.08	0.09	5.40	6.81	0.08	1.21
% C5	0.31	0.28	5.93	2.92	0.33	0.38	0.19	0.05	0.04	15.46
% C6	0.78	1.18	11.70	10.11	0.43	0.65	4.88	6.06	15.35	7.17
% C7	0.78	1.18	11.70	10.11	0.43	0.62	4.88	6.06	0.06	7.17
% C8	2.41	2.25	10.95	12.06	8.06	7.72	3.43	8.02	0.02	0.20
% C9	4.12	4.04	0.02	0.72	4.69	4.54	11.60	6.08	0.26	1.15
% C10	4.12	4.04	0.02	0.72	4.69	4.59	11.60	6.08	14.33	1.15
% C11	0.31	0.28	5.93	2.92	0.33	0.39	0.19	0.05	0.06	15.46
% C12	0.04	0.08	2.83	4.87	0.08	0.09	5.40	6.81	0.01	1.21
% C13	0.07	0.17	14.06	10.14	0.06	0.08	1.48	3.62	0.00	10.49
% C14	0.58	1.00	0.65	0.09	1.12	1.64	3.51	1.99	0.00	13.33
% O1	41.45	40.54	3.85	9.08	34.76	34.17	19.52	17.38	0.08	0.99
% O2	41.45	40.54	3.85	9.08	34.76	34.18	19.52	17.38	0.60	0.99

^aO = Occupied; V = Virtual (unoccupied)

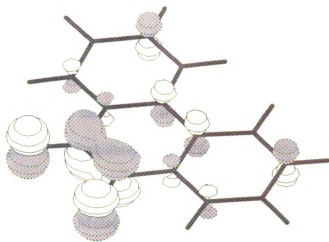


Figure 4.8. MO 55 α (HOMO) of phenanthrenesemiquinone. The orbital density lies above and below the plane of the ring.

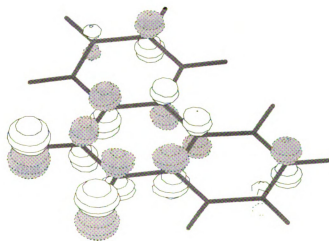


Figure 4.9. MO 55 β (LUMO) of phenanthrenesemiquinone. The orbital density lies above and below the plane of the ring.

semiquinone. For example, a comparison of Table 4.3 and Table 4.4 reveals that the orbital contributions to MO 52 from O1 and O2 increases from 5.49 % to approximately 41 % upon reduction of PhenQ to PhenSQ. Changes in percent contributions are also observed in other molecular orbitals. Since many of the physical properties of the quinone systems are linked to the HOMO, it is not clear how these changes might impact the behavior of the phenanthrenequinone (e.g., reactivity)

4.3.4. Energy Spacing of the Molecular Orbitals of PhenQ and PhenSQ

The absolute and relative orbital energies of PhenQ and PhenSQ are listed in Table 4.5. Since a direct comparison between the absolute energies of the orbitals of the two redox states is not possible due to the difference in the total electron count between the two molecules, only the relative energies of the orbitals will be examined.

In PhenQ the energy spacing between orbitals 52 α and 53 α is 0.644 eV. A much smaller energy difference of 0.018 eV is found between molecular orbitals 53 α and 54 α . The energy difference between MO 54 α and MO 55 α is 3.600 eV (HOMO-LUMO gap) which is larger than that found for 3,6-DTBQ of 3.230 eV for the HOMO-LUMO gap.¹⁸

Addition of an electron to PhenQ results in significant changes in the relative energy difference between the various molecular orbitals. Orbital 52 α is now just 0.179 eV below MO 53 α . In contrast, the energy spacing between MO 54 α and MO 55 α increases by ca. 0.66 eV. An increase is also observed in the energy spacing of MOs 55 α and 56 α . Molecular orbitals 54 α and 55 α , which correspond to the HOMO-LUMO gap in

Table 4.5. Absolute and Relative Orbital Energies (eV) of Phenanthrenequinone and Phenanthrenesemiquinone Calculated at the U-B3LYP/6-311G** Level

Orbital	PhenQ	PhenSQ
52 α	-7.515	-2.884
52 β	-7.515	-2.697
53 α	-6.871	-2.705
53 β	-6.871	-2.455
54 α	-6.853	-2.033
54 β	-6.853	-1.859
55 α	-3.253	-0.216
55 β	-3.253	1.542
56 α	-1.679	2.305
56 β	-1.679	2.386
53 α - 52 α	0.644	0.179
54 α - 53 α	0.019	0.672
55 α - 54 α	3.600 (LUMO – HOMO)	1.817
55 β - 55 α	0.000	1.758 (LUMO – HOMO)
56 α - 55 α	1.574	2.521

PhenQ, are separated by only 1.817 eV in PhenSQ. The HOMO-LUMO ($55\beta - 55\alpha$) gap in PhenSQ is only 1.817 eV which is substantially less than that observed in PhenQ.

4.3.5. Natural Population Analysis (NPA) Charge Densities and Spin Densities

The last characteristics to be considered are the charge and spin distributions of the ligand and how they change upon reduction. NPA charge densities of PhenQ and PhenSQ are tabulated in Table 4.6. Due to the difference in electronegativity between oxygen and carbon, we expected most of the negative charge density to reside on the oxygen atoms. This was precisely the result found from the analysis. For example, the negative charge density of PhenQ at O1 and O2 is -0.454 whereas the carbon atoms (except for C9 and C10) exhibit charge density values of less than -0.09 . Positive charge density is localized on the carbons atoms (C9 and C10) which are bonded to the oxygen atoms. This is expected due to the polarity of the C-O bond. The absolute charge densities of these carbon atoms are ca. $+0.414$. Upon reduction, the oxygen atoms experience an increase of approximately 0.10 in the magnitude of negative charge density. Most of the carbon atoms experience an increase in net negative charge (albeit less than the oxygen atoms), with the exception of C1 and C8 which exhibit a slight decrease in negative charge density. A significant decrease in positive charge density is observed for C9 and C10, although they maintain a net positive charge density of $+0.270$. These trends are in accord with what was found for reduction of 3,5-DTBQ and 3,6-DTBQ to the semiquinone redox states.¹⁸ However, the charge density found for the oxygen atoms in phenanthrenesemiquinone is approximately 0.1 less negative than

Table 4.6. NPA Atomic Charge Densities of Phenanthrenequinone and Phenanthrenesemiquinone Calculated at the U-B3LYP/6-311G** Level

Atom	PhenQ	PhenSQ
C1	-0.085	-0.065
C2	-0.020	-0.054
C3	-0.050	-0.089
C4	-0.039	-0.088
C5	-0.052	-0.073
C6	0.010	-0.018
C7	-0.003	-0.017
C8	-0.078	-0.066
C9	0.413	0.270
C10	0.415	0.269
C11	-0.057	-0.073
C12	-0.031	-0.088
C13	-0.052	-0.090
C14	-0.016	-0.054
O1	-0.454	-0.559
O2	-0.453	-0.559

either 3,5-DTBSQ or 3,6-DTBSQ. This indicates smaller net negative charge densities at the oxygen atoms of PhenSQ. It is interesting to speculate what this result may imply about reactivity, specifically in terms of a decrease in nucleophilicity relative to 3,5-DTBSQ.

Information on the spin densities of PhenSQ are listed in Table 4.7. The principle results found in the analysis of PhenSQ is that most of the spin density is located on O1 and O2. This result is in accord with what was found for 3,6-DTBQ and 3,6-DTBSQ.¹⁸ The Mulliken spin density values for O1 and O2 are 0.236 each. It appears as though the carbon atoms attached to the oxygen atoms have more spin density than the other carbon atoms; i.e., C9 and C10 have values of + 0.109. The finding that the majority of the spin density of PhenSQ resides on the oxygen atoms indicates that the mechanism for exchange in metal-phenanthrenesemiquinone complexes is likely to be direct exchange.

4.4. Concluding Remarks

Nonlocal gradient-correlated density functional theory was applied to the study of PhenQ and PhenSQ. The optimized geometry of PhenQ at the U-B3LYP/6-31G* level yielded a structure that is similar to the x-ray structure reported in the literature. Upon reduction of PhenQ to PhenSQ, single bonds contracted while double bonds elongated in accord with expectations from simple resonance pictures of the π system. For example, the C-O bond distances increase from a length characteristic of a double bond to one that is intermediate between a double bond and a single bond. This is in accord with what is expected for semiquinones.²⁹

Table 4.7. NPA Atomic Spin Densities and Mulliken Net Spin Densities for Phenanthrenequinone and Phenanthrenesemiquinone Obtained at the U-B3LYP/6-311G** Level

Atom	Mulliken Spin Densities	NPA Atomic Spin Densities
C1	0.031	0.035
C2	0.051	0.042
C3	0.008	0.010
C4	0.083	0.076
C5	-0.014	-0.015
C6	0.051	0.051
C7	0.052	0.052
C8	0.031	0.034
C9	0.109	0.105
C10	0.108	0.105
C11	-0.015	-0.016
C12	0.084	0.076
C13	0.007	0.009
C14	0.051	0.042
O1	0.236	0.238
O2	0.236	0.239

The electronic structures of PhenQ and PhenSQ were calculated at the U-B3LYP/6-311G** level using the optimized structures described above. The only similarities found between the molecular orbitals of PhenQ and PhenSQ is the HOMO of phenanthrenesemiquinone (MO 55 α) and MOs 55 α,β of phenanthrenequinone (LUMO). Hence, the Aufbau principle is applicable in the sense that the LUMO of PhenQ and the HOMO of PhenSQ are nearly identical in composition. The lower energy orbital compositions of PhenSQ differed substantially from PhenQ. This result is in contrast with what was found for the ligands, 3,5-DTBQ and 3,6-DTBQ.¹⁸ However, it is not clear if these differences are chemically significant because many of the physical properties of the quinone system are linked to the HOMO and not the lower energy orbitals.

Lastly, the natural population analysis (NPA) charge densities reveal that the majority of negative charge density resides on the oxygen atoms while the positive charge density resides on C9 and C10. This result signifies the polarity of the C-O bond and indicates the importance of electronegativity differences in the localization of net charge within the molecule. Overall, the negative charge density of the atoms increase upon reduction, with the oxygen atoms showing the largest increase. NPA atomic spin densities indicate that the unpaired spin density in PhenSQ is largely localized on the oxygen atoms. The remaining carbon atoms contain smaller non-zero values of spin density, with C9 and C10 having the largest values of + 0.109. This implies that the mechanism of exchange between phenanthrenesemiquinone and a metal ion is expected to be through direct exchange due to the localization of the majority of the spin density on the oxygen atoms which will be binding directly to the metal ion. It can be inferred that a Ni(II)-PhenSQ complex would be expected to exhibit ferromagnetic coupling due

to the fact that the σ -type magnetic orbitals of the Ni(II) ion are orthogonal to that of the semiquinone ligand. These implications can be further studied in future experiments on Ni(II)-SQ systems employing similar calculations.

4.5 Future Directions

A similar reaction (Reaction 2) outlined in Chapter 2 was applied to the synthesis of the $[\text{Ni}(\text{tren})(\text{PhenSQ})]^+$. However, the electronic spectrum of the material obtained matched that of PhenQ. This implies that either PhenSQ is not binding or that the product, $[\text{Ni}(\text{tren})(\text{PhenSQ})]^+$, is unstable and PhenSQ dissociates and/or oxidizes to the quinone redox state upon exposure to air. A problem encountered in this synthesis was the reduction of phenanthrenequinone to phenanthrenecatechol. It appears as though the reduction is not complete using either sodium metal or potassium metal. Due to this, the likely cause of the failed reaction is the binding of the semiquinone to the metal ion. A possible method to circumvent this is to oxidatively bind the quinone to a Ni complex (d^{10}) prior to any other steps. Another possible route that can be taken involves, first, making $\text{Ni}(\text{PMe}_3)_2(\text{PhenSQ})$ by the direct oxidative addition reaction between $\text{Ni}(\text{PMe}_3)_4$ and PhenQ.^{30,31} The next step would just involve the reaction of $\text{Ni}(\text{PMe}_3)_2(\text{PhenSQ})$ with tren, which should displace the trimethylphosphine ligands. The latter reaction is entropically favored and should proceed to yield $[\text{Ni}(\text{tren})(\text{PhenSQ})]$. This can then be oxidized to give $[\text{Ni}(\text{tren})(\text{PhenSQ})](\text{PF}_6)$ by stoichiometric addition of AgPF_6 .

Although it is not possible to formulate a direct comparison between the absolute energies of the orbitals of phenanthrenequinone, 3,5-DTBQ, and 3,6-DTBQ, the

qualitative differences in the localization of the molecular orbitals are noted above along with differences in the charge density localization. These dissimilarities are noteworthy and could be chemically significant. For example, we found that there was less negative charge density localization on the oxygen atoms of PhenSQ than either 3,5-DTBSQ or 3,6-DTBSQ. This result explains and supports our finding that the phenanthrenesemiquinone ligand exhibits weaker binding affinity to metal centers.

4.5. References

- (1) *The Chemistry of the Quinonoid Compounds*; Wiley: New York, 1974.
- (2) Wheeler, D. E.; Mccusker, J. K. *Inorg. Chem.* **1998**, *37*, 2296.
- (3) Benelli, C.; Dei, A.; Gatteschi, D.; Pardi, L. *Inorg. Chem.* **1990**, *29*, 3409.
- (4) Lange, C. W.; Conklin, B. J.; Pierpont, C. G. *Inorg. Chem.* **1994**, *33*, 1276.
- (5) Benelli, C.; Dei, A.; Gatteschi, D.; Pardi, L. *Inorg. Chem.* **1988**, *27*, 2831.
- (6) Benelli, C.; Dei, A.; Gatteschi, D.; Güdel, H. U.; Pardi, L. *Inorg. Chem.* **1989**, *28*, 3089.
- (7) Buchanan, R. M.; Claflin, J.; Pierpont, C. G. *Inorg. Chem.* **1983**, *22*, 2552.
- (8) Kessel, S. L.; Emberson, R. M.; Debrunner, P. G.; Hendrickson, D. N. *Inorg. Chem.* **1980**, *19*, 1170.
- (9) Attia, A. S.; Pierpont, C. G. *Inorg. Chem.* **1995**, *34*, 1172.
- (10) Attia, A. S.; Pierpont, C. G. *Inorg. Chem.* **1997**, *36*, 6184.
- (11) Attia, A. S.; Bhattacharya, S.; Pierpont, C. G. *Inorg. Chem.* **1995**, *34*, 4427.
- (12) Kahn, O.; Prins, R.; Redijk, J.; Thompson, J. *Inorg. Chem.* **1987**, *26*, 3557.
- (13) Ruf, M.; Noll, B. C.; Groner, M. D.; Yee, G. T.; Pierpont, C. G. *Inorg. Chem.* **1997**, *36*, 4860.
- (14) Gordon, D. J.; Fenske, R. F. *Inorg. Chem.* **1982**, *21*, 2907.
- (15) Gordon, D. J.; Fenske, R. F. *Inorg. Chem.* **1982**, *21*, 2916.
- (16) Rodriguez, J. H.; Wheeler, D. E.; Mccusker, J. K. *J. Am. Chem. Soc.* **1998**, *120*, 12051.

- (17) Bianchini, C.; Masi, D.; Mealli, C.; Meli, A.; Martini, G.; Laschi, F.; Zanello, P. *Inorg. Chem.* **1987**, *26*, 3683.
- (18) Wheeler, D. E.; Rodriguez, J. H.; Mccusker, J. K. *J. Phys. Chem.* **1999**, *103*, 4101.
- (19) Frisch, M. J.; Trucks, G. W.; Schlegel, H. B.; Scuseria, G. E.; Robb, M. A.; Cheeseman, J. R.; Zakrzewski, V. G.; Montgomery, J. A.; Stratmann, R. E.; Burant, J. C.; Dapprich, S.; Millam, J. M.; Daniels, A. D.; Kudin, K. N.; Strain, M. C.; Farkas, O.; Tomasi, J.; Barone, V.; Cossi, M.; Cammi, R.; Mennucci, B.; Pomelli, C.; Adamo, C.; Clifford, S.; Ochterski, J.; Petersson, G. A.; Ayala, P. Y.; Cui, Q.; Morokuma, K.; Malick, D. K.; Rabuck, A. D.; Raghavachari, K.; Foresman, J. B.; Cioslowski, J.; Ortiz, J. V.; Stefanov, B. B.; Liu, G.; Liashenko, A.; Piskorz, P.; Komaromi, I.; Gomperts, R.; Martin, R. L.; Fox, D. J.; Keith, T.; Al-Laham, M. A.; Peng, C. Y.; Nanayakkara, A.; Gonzalez, C.; Challacombe, M.; Gill, P. M. W.; Johnson, B.; Chen, W.; Wong, M. W.; Andres, J. L.; Gonzalez, C.; Head-Gordon, M.; Replogle, E. S.; Pople, J. A. *Gaussian 98*, revision A.4; Gaussian, Inc.: Pittsburgh, PA, 1998.
- (20) Lee, C.; Yang, W.; Parr, R. G. *Phys. Rev. B* **1988**, *37*, 785.
- (21) Becke, A. D. *Phys. Rev. A* **1988**, *38*, 3098.
- (22) Becke, A. D. *J. Chem. Phys.* **1993**, *98*, 1372.
- (23) Becke, A. D. *J. Chem. Phys.* **1993**, *98*, 5648.
- (24) Frisch, M. J.; Frisch, A. *Gaussian 98 User's Reference*; Gaussian, Inc.: Pittsburgh, 1998.
- (25) Reed, A. E.; Wienhold, R. J. *J. Chem. Phys.* **1983**, *78*, 4066.

- (26) Reed, A. E.; Weinstock, R. B.; Wienhold, R. J. *J. Chem. Phys.* **1985**, *83*, 735.
- (27) Glendening, E. D.; Reed, A. E.; Carpenter, J. E.; Weinhold, F. *NBO 3.1*, Theoretical Chemistry Institute, University of Wisconsin: Madison, WI, 1996.
- (28) Matsuzaki, S. Y.; Gotoh, M.; Kuboyama, A. *Mol. Cryst. Liq. Crst.* **1987**, *142*, 127.
- (29) Pierpont, C. G.; Attia, A. S. *Collect. Czech. Chem. Commun.* **2001**, *66*, 33.
- (30) Klein, H. F.; Karsch, H. H. *Chem. Ber.* **1976**, *109*, 2515.
- (31) Klein, H. F.; Auer, E.; Dal, A.; Lemke, U.; Lemke, M.; Jung, T.; Rohr, C.; Florke, U.; Haupt, H. *Inorg. Chim. Acta* **1999**, *287*, 167.

Appendix

Tables of Bond Lengths, Bond Angles, and Anisotropic Thermal Factors

for the Crystal Structure of [Ni(tren)(3,5-DTBSQ)](PF₆)

Presented in Chapter 2

Table A.1. Bond Distances (Å) for [Ni(tren)(3,5-DTBSQ)](PF₆)

Bond	Bond Distance (Å)	Bond	Bond Distance (Å)
Ni(1)-O(2)	2.022(2)	N(1)-C(15)	1.53(3)
Ni(1)-N(2)	2.032(19)	N(3)-C(18)	1.471(5)
Ni(1)-O(1)	2.085(3)	N(4)-C(20)	1.488(5)
Ni(1)-N(1)	2.091(3)	N(2)-C(16)	1.49(2)
Ni(1)-N(3)	2.113(3)	C(15)-C(16)	1.57(3)
Ni(1)-N(4)	2.120(3)	N(2')-C(16')	1.42(2)
Ni(1)-N(2')	2.136(17)	C(15')-C(16')	1.48(3)
O(1)-C(1)	1.286(4)	C(17)-C(18)	1.513(6)
O(2)-C(2)	1.279(4)	C(19)-C(20)	1.511(5)
C(1)-C(6)	1.415(5)	Ni(2)-O(12)	2.025(2)
C(1)-C(2)	1.458(5)	Ni(2)-O(11)	2.079(2)
C(2)-C(3)	1.438(5)	Ni(2)-N(14)	2.086(3)
C(3)-C(4)	1.372(5)	Ni(2)-N(11)	2.088(3)
C(3)-C(7)	1.535(5)	Ni(2)-N(12)	2.099(3)
C(4)-C(5)	1.430(5)	Ni(2)-N(13)	2.119(3)
C(5)-C(6)	1.369(5)	O(11)-C(21)	1.294(4)
C(5)-C(11)	1.532(5)	O(12)-C(22)	1.278(4)
C(7)-C(10)	1.534(5)	C(21)-C(26)	1.412(5)
C(7)-C(8)	1.540(5)	C(21)-C(22)	1.468(5)
C(7)-C(9)	1.541(5)	C(22)-C(23)	1.453(5)
C(11)-C(13)	1.525(5)	C(23)-C(24)	1.363(5)
C(11)-C(12)	1.531(6)	C(23)-C(27)	1.526(5)
C(11)-C(14)	1.533(5)	C(24)-C(25)	1.429(5)
N(1)-C(15')	1.44(3)	C(25)-C(26)	1.371(5)
N(1)-C(17)	1.484(5)	C(25)-C(31)	1.539(5)
N(1)-C(19)	1.489(5)	C(27)-C(30)	1.531(5)

Table A.1. continued

Bond	Bond Distance (Å)	Bond	Bond Distance (Å)
C(27)-C(28)	1.536(6)	P(2)-F(13)	1.556(13)
C(27)-C(29)	1.538(6)	P(2)-F(15)	1.561(13)
C(31)-C(34)	1.522(5)	P(2)-F(12')	1.569(9)
C(31)-C(32)	1.525(6)	P(2)-F(11')	1.572(15)
C(31)-C(33)	1.526(6)	P(2)-F(16')	1.659(8)
N(11)-C(37)	1.470(5)	P(2)-F(11)	1.747(10)
N(11)-C(35)	1.482(5)	F(11)-F(13')	1.56(2)
N(11)-C(39)	1.483(5)	F(11)-F(14')	1.64(2)
N(12)-C(36)	1.483(6)	F(11)-F(14)	1.703(17)
N(13)-C(38)	1.475(5)	F(12)-F(15')	1.22(3)
N(14)-C(40)	1.476(7)	F(12)-F(12')	1.23(3)
C(35)-C(36)	1.517(7)	F(12)-F(16)	1.78(3)
C(37)-C(38)	1.505(6)	F(13)-F(13')	0.71(3)
C(39)-C(40)	1.477(7)	F(13)-F(16')	1.78(2)
P(1)-F(3)	1.557(3)	F(14)-F(12')	1.17(2)
P(1)-F(2)	1.560(3)	F(14)-F(11')	1.28(2)
P(1)-F(1)	1.564(4)	F(15)-F(15')	1.18(3)
P(1)-F(5)	1.567(3)	F(15)-F(11')	1.29(3)
P(1)-F(6)	1.583(3)	F(16)-F(14')	0.62(2)
P(1)-F(4)	1.598(3)	F(16)-F(16')	1.57(2)
P(2)-F(16)	1.392(14)	F(11')-F(13')	1.78(2)
P(2)-F(15')	1.426(16)	F(15')-F(16')	1.58(2)
P(2)-F(13')	1.432(12)	O(51)-C(52)	1.197(6)
P(2)-F(14)	1.494(11)	O(52)-C(52)	1.322(6)
P(2)-F(12)	1.540(14)	O(52)-C(53)	1.472(7)
P(2)-F(14')	1.553(13)	C(51)-C(52)	1.466(8)

Table A.1. continued

Bond	Bond Distance (Å)	Bond	Bond Distance (Å)
C(53)-C(54)	1.322(11)	O(54)-C(57)	1.425(12)
O(53)-C(56)	1.206(6)	C(57)-C(58)	1.483(16)
C(55)-C(56)	1.473(7)	O(54')-C(57')	1.72(6)
C(56)-O(54')	1.30(2)	C(57')-C(58')	1.39(6)
C(56)-O(54)	1.355(9)		

Table A.2. Bond Angles (°) for [Ni(tren)(3,5-DTBSQ)](PF₆)

Atoms	Angle	Atoms	Angle
O(2)-Ni(1)-N(2)	95.8(6)	O(2)-C(2)-C(3)	123.8(3)
O(2)-Ni(1)-O(1)	80.49(9)	O(2)-C(2)-C(1)	117.4(3)
N(2)-Ni(1)-O(1)	175.7(6)	C(3)-C(2)-C(1)	118.8(3)
O(2)-Ni(1)-N(1)	177.64(11)	C(4)-C(3)-C(2)	117.8(3)
N(2)-Ni(1)-N(1)	83.2(6)	C(4)-C(3)-C(7)	122.4(3)
O(1)-Ni(1)-N(1)	100.54(11)	C(2)-C(3)-C(7)	119.8(3)
O(2)-Ni(1)-N(3)	94.62(11)	C(3)-C(4)-C(5)	124.1(3)
N(2)-Ni(1)-N(3)	95.6(6)	C(6)-C(5)-C(4)	118.5(3)
O(1)-Ni(1)-N(3)	86.94(11)	C(6)-C(5)-C(11)	122.7(3)
N(1)-Ni(1)-N(3)	83.33(12)	C(4)-C(5)-C(11)	118.8(3)
O(2)-Ni(1)-N(4)	99.37(11)	C(5)-C(6)-C(1)	121.0(3)
N(2)-Ni(1)-N(4)	94.7(5)	C(10)-C(7)-C(3)	112.5(3)
O(1)-Ni(1)-N(4)	83.77(11)	C(10)-C(7)-C(8)	107.2(3)
N(1)-Ni(1)-N(4)	82.87(12)	C(3)-C(7)-C(8)	109.5(3)
N(3)-Ni(1)-N(4)	161.66(12)	C(10)-C(7)-C(9)	107.5(3)
O(2)-Ni(1)-N(2')	94.8(7)	C(3)-C(7)-C(9)	109.9(3)
N(2)-Ni(1)-N(2')	1.0(13)	C(8)-C(7)-C(9)	110.3(3)
O(1)-Ni(1)-N(2')	174.7(7)	C(13)-C(11)-C(12)	108.3(3)
N(1)-Ni(1)-N(2')	84.3(7)	C(13)-C(11)-C(5)	110.0(3)
N(3)-Ni(1)-N(2')	95.8(6)	C(12)-C(11)-C(5)	111.7(3)
N(4)-Ni(1)-N(2')	94.8(6)	C(13)-C(11)-C(14)	109.0(3)
C(1)-O(1)-Ni(1)	110.6(2)	C(12)-C(11)-C(14)	107.9(3)
C(2)-O(2)-Ni(1)	113.3(2)	C(5)-C(11)-C(14)	109.8(3)
O(1)-C(1)-C(6)	122.1(3)	C(15')-N(1)-C(17)	115.1(13)
O(1)-C(1)-C(2)	118.1(3)	C(15')-N(1)-C(19)	113.0(11)
C(6)-C(1)-C(2)	119.7(3)	C(17)-N(1)-C(19)	112.1(3)

Table A.2. continued

Atoms	Angle	Atoms	Angle
C(15')-N(1)-C(15)	9(3)	O(11)-Ni(2)-N(12)	88.60(12)
C(17)-N(1)-C(15)	109.3(12)	N(14)-Ni(2)-N(12)	93.80(14)
C(19)-N(1)-C(15)	110.7(11)	N(11)-Ni(2)-N(12)	82.77(13)
C(15')-N(1)-Ni(1)	104.4(14)	O(12)-Ni(2)-N(13)	98.82(12)
C(17)-N(1)-Ni(1)	105.6(2)	O(11)-Ni(2)-N(13)	85.16(12)
C(19)-N(1)-Ni(1)	105.6(2)	N(14)-Ni(2)-N(13)	92.91(14)
C(15)-N(1)-Ni(1)	113.5(13)	N(11)-Ni(2)-N(13)	83.11(13)
C(18)-N(3)-Ni(1)	109.9(2)	N(12)-Ni(2)-N(13)	163.61(13)
C(20)-N(4)-Ni(1)	110.1(2)	C(21)-O(11)-Ni(2)	111.3(2)
C(16)-N(2)-Ni(1)	110.4(12)	C(22)-O(12)-Ni(2)	113.3(2)
N(1)-C(15)-C(16)	107(2)	O(11)-C(21)-C(26)	123.0(3)
N(2)-C(16)-C(15)	111.9(15)	O(11)-C(21)-C(22)	117.0(3)
C(16')-N(2')-Ni(1)	106.7(11)	C(26)-C(21)-C(22)	120.0(3)
N(1)-C(15')-C(16')	119(2)	O(12)-C(22)-C(23)	123.7(3)
N(2')-C(16')-C(15')	108.2(17)	O(12)-C(22)-C(21)	117.8(3)
N(1)-C(17)-C(18)	111.0(3)	C(23)-C(22)-C(21)	118.5(3)
N(3)-C(18)-C(17)	109.6(3)	C(24)-C(23)-C(22)	117.1(3)
N(1)-C(19)-C(20)	110.7(3)	C(24)-C(23)-C(27)	123.6(3)
N(4)-C(20)-C(19)	109.9(3)	C(22)-C(23)-C(27)	119.4(3)
O(12)-Ni(2)-O(11)	80.52(9)	C(23)-C(24)-C(25)	125.1(3)
O(12)-Ni(2)-N(14)	97.78(12)	C(26)-C(25)-C(24)	118.6(3)
O(11)-Ni(2)-N(14)	177.18(12)	C(26)-C(25)-C(31)	123.0(3)
O(12)-Ni(2)-N(11)	177.43(11)	C(24)-C(25)-C(31)	118.4(3)
O(11)-Ni(2)-N(11)	98.00(11)	C(25)-C(26)-C(21)	120.7(3)
N(14)-Ni(2)-N(11)	83.78(13)	C(23)-C(27)-C(30)	111.6(3)
O(12)-Ni(2)-N(12)	95.07(12)	C(23)-C(27)-C(28)	110.3(3)

Table A.2. continued

Atoms	Angle	Atoms	Angle
C(30)-C(27)-C(28)	107.9(4)	F(3)-P(1)-F(1)	179.1(3)
C(23)-C(27)-C(29)	109.6(3)	F(2)-P(1)-F(1)	89.2(3)
C(30)-C(27)-C(29)	107.8(3)	F(3)-P(1)-F(5)	90.2(2)
C(28)-C(27)-C(29)	109.6(3)	F(2)-P(1)-F(5)	91.73(19)
C(34)-C(31)-C(32)	109.6(4)	F(1)-P(1)-F(5)	90.6(3)
C(34)-C(31)-C(33)	107.2(4)	F(3)-P(1)-F(6)	90.0(2)
C(32)-C(31)-C(33)	107.6(4)	F(2)-P(1)-F(6)	177.16(19)
C(34)-C(31)-C(25)	110.2(3)	F(1)-P(1)-F(6)	89.5(2)
C(32)-C(31)-C(25)	110.1(3)	F(5)-P(1)-F(6)	90.82(17)
C(33)-C(31)-C(25)	112.1(3)	F(3)-P(1)-F(4)	89.2(2)
C(37)-N(11)-C(35)	111.8(3)	F(2)-P(1)-F(4)	88.23(18)
C(37)-N(11)-C(39)	111.4(3)	F(1)-P(1)-F(4)	90.0(2)
C(35)-N(11)-C(39)	113.6(3)	F(5)-P(1)-F(4)	179.4(2)
C(37)-N(11)-Ni(2)	105.6(2)	F(6)-P(1)-F(4)	89.23(16)
C(35)-N(11)-Ni(2)	104.1(2)	F(16)-P(2)-F(15')	93.1(14)
C(39)-N(11)-Ni(2)	109.8(2)	F(16)-P(2)-F(13')	103.8(12)
C(36)-N(12)-Ni(2)	110.6(2)	F(15')-P(2)-F(13')	136.4(17)
C(38)-N(13)-Ni(2)	109.3(2)	F(16)-P(2)-F(14)	128.0(16)
C(40)-N(14)-Ni(2)	105.6(3)	F(15')-P(2)-F(14)	110.7(10)
N(11)-C(35)-C(36)	110.0(4)	F(13')-P(2)-F(14)	90.0(13)
N(12)-C(36)-C(35)	109.1(3)	F(16)-P(2)-F(12)	74.4(12)
N(11)-C(37)-C(38)	111.0(3)	F(15')-P(2)-F(12)	48.6(11)
N(13)-C(38)-C(37)	110.0(3)	F(13')-P(2)-F(12)	175(2)
C(40)-C(39)-N(11)	111.9(4)	F(14)-P(2)-F(12)	87.6(9)
C(39)-C(40)-N(14)	112.8(4)	F(16)-P(2)-F(14')	23.5(9)
F(3)-P(1)-F(2)	91.2(2)	F(15')-P(2)-F(14')	115.8(14)

Table A.2. continued

Atoms	Angle	Atoms	Angle
F(13')-P(2)-F(14')	89.9(10)	F(13')-P(2)-F(11')	72.4(9)
F(14)-P(2)-F(14')	110.2(12)	F(14)-P(2)-F(11')	49.2(10)
F(12)-P(2)-F(14')	86.9(14)	F(12)-P(2)-F(11')	109.1(9)
F(16)-P(2)-F(13)	98.0(13)	F(14')-P(2)-F(11')	151.2(16)
F(15')-P(2)-F(13)	111.6(14)	F(13)-P(2)-F(11')	80.4(10)
F(13')-P(2)-F(13)	27.3(11)	F(15)-P(2)-F(11')	48.7(11)
F(14)-P(2)-F(13)	113.4(15)	F(12')-P(2)-F(11')	86.4(9)
F(12)-P(2)-F(13)	156.9(17)	F(16)-P(2)-F(16')	61.1(10)
F(14')-P(2)-F(13)	94.3(8)	F(15')-P(2)-F(16')	60.9(9)
F(16)-P(2)-F(15)	136.5(10)	F(13')-P(2)-F(16')	92.8(8)
F(15')-P(2)-F(15)	46.2(10)	F(14)-P(2)-F(16')	169.5(8)
F(13')-P(2)-F(15)	100.0(13)	F(12)-P(2)-F(16')	90.4(13)
F(14)-P(2)-F(15)	87.4(8)	F(14')-P(2)-F(16')	80.0(7)
F(12)-P(2)-F(15)	84.3(14)	F(13)-P(2)-F(16')	67.2(8)
F(14')-P(2)-F(15)	159.9(10)	F(15)-P(2)-F(16')	82.1(6)
F(13)-P(2)-F(15)	87.0(9)	F(12')-P(2)-F(16')	136.3(10)
F(16)-P(2)-F(12')	93.4(14)	F(11')-P(2)-F(16')	122.3(17)
F(15')-P(2)-F(12')	88.4(9)	F(16)-P(2)-F(11)	82.8(7)
F(13')-P(2)-F(12')	129.3(12)	F(15')-P(2)-F(11)	165.8(13)
F(14)-P(2)-F(12')	44.6(8)	F(13')-P(2)-F(11)	57.7(10)
F(12)-P(2)-F(12')	46.8(9)	F(14)-P(2)-F(11)	62.8(6)
F(14')-P(2)-F(12')	87.9(8)	F(12)-P(2)-F(11)	117.3(18)
F(13)-P(2)-F(12')	156.3(12)	F(14')-P(2)-F(11)	59.3(7)
F(15)-P(2)-F(12')	99.0(7)	F(13)-P(2)-F(11)	82.5(8)
F(16)-P(2)-F(11')	174.6(15)	F(15)-P(2)-F(11)	140.5(9)
F(15')-P(2)-F(11')	92.2(11)	F(12')-P(2)-F(11)	78.4(6)

Table A.2. continued

Atoms	Angle	Atoms	Angle
F(11')-P(2)-F(11)	91.9(15)	F(14')-F(16)-P(2)	93(3)
F(16')-P(2)-F(11)	126.9(5)	F(14')-F(16)-F(16')	137(4)
F(13')-F(11)-F(14')	82.5(8)	P(2)-F(16)-F(16')	67.9(9)
F(13')-F(11)-F(14)	78.6(11)	F(14')-F(16)-F(12)	117(4)
F(14')-F(11)-F(14)	96.7(10)	P(2)-F(16)-F(12)	56.6(8)
F(13')-F(11)-P(2)	50.9(5)	F(16')-F(16)-F(12)	85.3(16)
F(14')-F(11)-P(2)	54.5(5)	F(14)-F(11')-F(15)	110.4(17)
F(14)-F(11)-P(2)	51.3(4)	F(14)-F(11')-P(2)	62.2(9)
F(15')-F(12)-F(12')	116.4(19)	F(15)-F(11')-P(2)	65.2(11)
F(15')-F(12)-P(2)	60.8(11)	F(14)-F(11')-F(13')	83.5(14)
F(12')-F(12)-P(2)	67.8(11)	F(15)-F(11')-F(13')	95.4(19)
F(15')-F(12)-F(16)	83.9(14)	P(2)-F(11')-F(13')	50.2(6)
F(12')-F(12)-F(16)	90(2)	F(14)-F(12')-F(12)	122.0(15)
P(2)-F(12)-F(16)	49.0(8)	F(14)-F(12')-P(2)	64.3(7)
F(13')-F(13)-P(2)	66.7(16)	F(12)-F(12')-P(2)	65.4(8)
F(13')-F(13)-F(16')	122(2)	F(13)-F(13')-P(2)	86(2)
P(2)-F(13)-F(16')	59.2(7)	F(13)-F(13')-F(11)	145(3)
F(12')-F(14)-F(11')	123(2)	P(2)-F(13')-F(11)	71.4(9)
F(12')-F(14)-P(2)	71.1(10)	F(13)-F(13')-F(11')	99(3)
F(11')-F(14)-P(2)	68.6(12)	P(2)-F(13')-F(11')	57.5(7)
F(12')-F(14)-F(11)	92.2(17)	F(11)-F(13')-F(11')	91.2(16)
F(11')-F(14)-F(11)	105.7(14)	F(16)-F(14')-P(2)	64(2)
P(2)-F(14)-F(11)	65.9(7)	F(16)-F(14')-F(11)	130(3)
F(15')-F(15)-F(11')	122.2(18)	P(2)-F(14')-F(11)	66.3(8)
F(15')-F(15)-P(2)	60.8(10)	F(15)-F(15')-F(12)	120(3)
F(11')-F(15)-P(2)	66.1(9)	F(15)-F(15')-P(2)	73.0(16)

Table A.2. continued

Atoms	Angle	Atoms	Angle
F(12)-F(15')-P(2)	70.6(14)	O(52)-C(52)-C(51)	112.0(5)
F(15)-F(15')-F(16')	99(2)	C(54)-C(53)-O(52)	112.5(7)
F(12)-F(15')-F(16')	107.7(15)	O(53)-C(56)-O(54')	120.5(12)
P(2)-F(15')-F(16')	66.9(9)	O(53)-C(56)-O(54)	121.9(6)
F(16)-F(16')-F(15')	81.3(11)	O(54')-C(56)-O(54)	31(3)
F(16)-F(16')-P(2)	51.0(6)	O(53)-C(56)-C(55)	125.7(5)
F(15')-F(16')-P(2)	52.2(6)	O(54')-C(56)-C(55)	108.6(11)
F(16)-F(16')-F(13)	83.2(9)	O(54)-C(56)-C(55)	112.0(5)
F(15')-F(16')-F(13)	94.4(13)	C(56)-O(54)-C(57)	117.8(7)
P(2)-F(16')-F(13)	53.6(5)	O(54)-C(57)-C(58)	115.1(9)
C(52)-O(52)-C(53)	113.4(5)	C(56)-O(54')-C(57')	114(2)
O(51)-C(52)-O(52)	123.5(6)	C(58')-C(57')-O(54')	82(4)
O(51)-C(52)-C(51)	124.4(6)		

Table A.3. Anisotropic Displacement Parameters [$\text{\AA}^2 \times 10^3$] for [Ni(tren)(3,5-DTBSQ)](PF₆). The Anisotropic Displacement Factor Exponent Takes the Form: $-2p^2 [(ha^*)^2U_{11} + \dots + 2hka^*b^*U_{12}]$

Atom	U11	U22	U33	U23	U13	U12
Ni(1)	26(1)	30(1)	19(1)	4(1)	4(1)	1(1)
O(1)	30(1)	38(2)	23(1)	6(1)	3(1)	-2(1)
O(2)	29(1)	31(1)	23(1)	3(1)	3(1)	-4(1)
C(1)	27(2)	25(2)	20(2)	3(2)	5(2)	5(2)
C(2)	27(2)	26(2)	23(2)	3(2)	4(2)	6(2)
C(3)	28(2)	28(2)	23(2)	7(2)	5(2)	5(2)
C(4)	29(2)	35(2)	24(2)	10(2)	7(2)	6(2)
C(5)	25(2)	30(2)	25(2)	4(2)	0(2)	10(2)
C(6)	21(2)	30(2)	27(2)	4(2)	1(2)	1(2)
C(7)	33(2)	35(2)	24(2)	8(2)	3(2)	-3(2)
C(8)	32(2)	45(2)	43(2)	10(2)	8(2)	1(2)
C(9)	40(2)	31(2)	45(3)	9(2)	3(2)	-1(2)
C(10)	44(3)	53(3)	39(2)	13(2)	13(2)	-13(2)
C(11)	31(2)	37(2)	20(2)	0(2)	-2(2)	6(2)
C(12)	38(2)	66(3)	29(2)	-4(2)	-3(2)	-9(2)
C(13)	60(3)	52(3)	27(2)	1(2)	-6(2)	23(2)
C(14)	44(2)	44(2)	35(2)	-6(2)	2(2)	8(2)
N(1)	26(2)	30(2)	21(2)	1(1)	2(1)	1(1)
N(3)	32(2)	40(2)	28(2)	1(2)	6(1)	8(2)
N(4)	36(2)	34(2)	31(2)	5(1)	-2(1)	3(1)
N(2)	29(10)	55(13)	40(13)	30(9)	19(8)	16(8)
C(15)	25(9)	27(8)	9(8)	5(7)	-1(5)	-13(5)
C(16)	38(6)	44(6)	23(4)	-4(4)	5(4)	-4(5)
N(2')	34(11)	12(8)	24(11)	-24(6)	-8(7)	-15(6)
C(15')	56(14)	45(13)	23(11)	17(7)	22(7)	20(10)
C(16')	26(6)	46(6)	26(5)	5(4)	2(4)	-1(4)

Table A.3. continued

Atom	U11	U22	U33	U23	U13	U12
C(17)	45(3)	32(2)	37(2)	8(2)	9(2)	2(2)
C(18)	56(3)	37(2)	33(2)	8(2)	9(2)	15(2)
C(19)	25(2)	44(2)	39(2)	9(2)	8(2)	3(2)
C(20)	30(2)	46(2)	42(2)	7(2)	8(2)	12(2)
Ni(2)	25(1)	32(1)	21(1)	4(1)	3(1)	5(1)
O(11)	30(1)	38(2)	26(1)	5(1)	4(1)	11(1)
O(12)	36(2)	39(2)	22(1)	8(1)	2(1)	14(1)
C(21)	23(2)	25(2)	25(2)	4(2)	5(2)	1(2)
C(22)	21(2)	24(2)	26(2)	3(2)	3(2)	0(2)
C(23)	26(2)	29(2)	27(2)	4(2)	5(2)	6(2)
C(24)	34(2)	37(2)	20(2)	4(2)	7(2)	9(2)
C(25)	25(2)	28(2)	25(2)	5(2)	0(2)	-1(2)
C(26)	19(2)	29(2)	32(2)	7(2)	3(2)	5(2)
C(27)	42(2)	36(2)	26(2)	5(2)	6(2)	17(2)
C(28)	32(2)	51(3)	55(3)	15(2)	8(2)	15(2)
C(29)	45(3)	36(2)	49(3)	7(2)	-2(2)	14(2)
C(30)	71(3)	70(3)	42(3)	11(2)	16(2)	47(3)
C(31)	25(2)	46(2)	26(2)	14(2)	3(2)	6(2)
C(32)	69(3)	69(3)	27(2)	16(2)	-15(2)	-16(3)
C(33)	73(3)	95(4)	39(3)	30(3)	10(2)	51(3)
C(34)	36(2)	82(3)	50(3)	37(3)	4(2)	0(2)
N(11)	32(2)	36(2)	30(2)	4(1)	8(1)	4(1)
N(12)	30(2)	54(2)	36(2)	10(2)	5(2)	-3(2)
N(13)	37(2)	38(2)	39(2)	8(2)	-5(2)	-4(2)
N(14)	41(2)	56(2)	35(2)	14(2)	6(2)	16(2)
C(35)	67(3)	30(2)	49(3)	-1(2)	26(2)	8(2)

Table A.3. continued

Atom	U11	U22	U33	U23	U13	U12
C(36)	72(3)	44(3)	46(3)	-2(2)	14(2)	-19(2)
C(37)	34(2)	52(3)	54(3)	16(2)	17(2)	14(2)
C(38)	28(2)	57(3)	60(3)	18(2)	9(2)	-3(2)
C(39)	56(3)	57(3)	29(2)	4(2)	12(2)	8(2)
C(40)	105(5)	126(5)	43(3)	24(3)	1(3)	61(4)
P(1)	29(1)	39(1)	43(1)	4(1)	6(1)	5(1)
F(1)	136(4)	202(5)	111(3)	103(3)	13(3)	67(3)
F(2)	97(3)	96(3)	114(3)	-40(2)	57(2)	2(2)
F(3)	84(2)	119(3)	117(3)	71(2)	5(2)	39(2)
F(4)	54(2)	60(2)	118(3)	-10(2)	36(2)	-16(1)
F(5)	52(2)	87(2)	106(3)	-16(2)	13(2)	-27(2)
F(6)	61(2)	62(2)	91(2)	-12(2)	39(2)	6(1)
P(2)	34(1)	60(1)	141(2)	32(1)	1(1)	8(1)
F(11)	88(7)	160(10)	148(11)	78(9)	48(6)	45(6)
F(12)	153(15)	320(30)	230(20)	-86(18)	-16(13)	166(18)
F(13)	82(8)	80(7)	350(30)	74(13)	3(12)	50(6)
F(14)	91(9)	320(30)	139(13)	162(17)	-4(9)	41(14)
F(15)	74(7)	134(11)	160(13)	86(11)	0(8)	-22(7)
F(16)	178(15)	250(20)	84(8)	-30(10)	25(8)	-151(14)
F(11')	90(8)	144(13)	430(30)	-139(17)	52(16)	-28(9)
F(12')	60(5)	126(9)	223(17)	115(11)	59(9)	51(6)
F(13')	87(8)	340(30)	117(10)	-50(13)	30(7)	63(13)
F(14')	108(8)	87(6)	260(20)	58(10)	55(10)	-32(6)
F(15')	184(19)	300(30)	250(20)	210(20)	76(16)	-44(17)
F(16')	80(6)	191(11)	127(9)	74(8)	-45(6)	-17(6)
O(51)	138(4)	93(3)	54(3)	36(2)	-19(2)	-52(3)

Table A.3. continued

Atom	U11	U22	U33	U23	U13	U12
O(52)	54(2)	66(2)	65(2)	14(2)	-1(2)	-3(2)
C(51)	61(3)	59(3)	99(5)	29(3)	-24(3)	-7(3)
C(52)	63(3)	49(3)	61(4)	22(3)	-15(3)	-23(3)
C(53)	81(5)	101(5)	116(6)	0(5)	19(4)	4(4)
C(54)	106(7)	197(11)	400(20)	-189(12)	-122(10)	88(8)
O(53)	111(3)	76(2)	46(2)	4(2)	19(2)	49(2)
C(55)	80(4)	79(4)	80(4)	39(3)	26(3)	37(3)
C(56)	66(3)	72(3)	39(3)	11(3)	10(2)	30(3)
O(54)	23(4)	39(3)	35(3)	2(2)	3(2)	8(2)
C(57)	49(5)	29(6)	40(5)	3(3)	3(4)	11(4)
C(58)	39(6)	59(7)	41(5)	15(4)	12(4)	13(5)
O(54')	460(50)	100(17)	60(13)	35(12)	100(20)	150(30)
C(57')	100(20)	190(40)	110(20)	60(20)	55(17)	30(20)
C(58')	260(60)	22(14)	490(90)	30(20)	300(60)	20(20)

MICHIGAN STATE UNIVERSITY LIBRARIES



3 1293 02372 0869